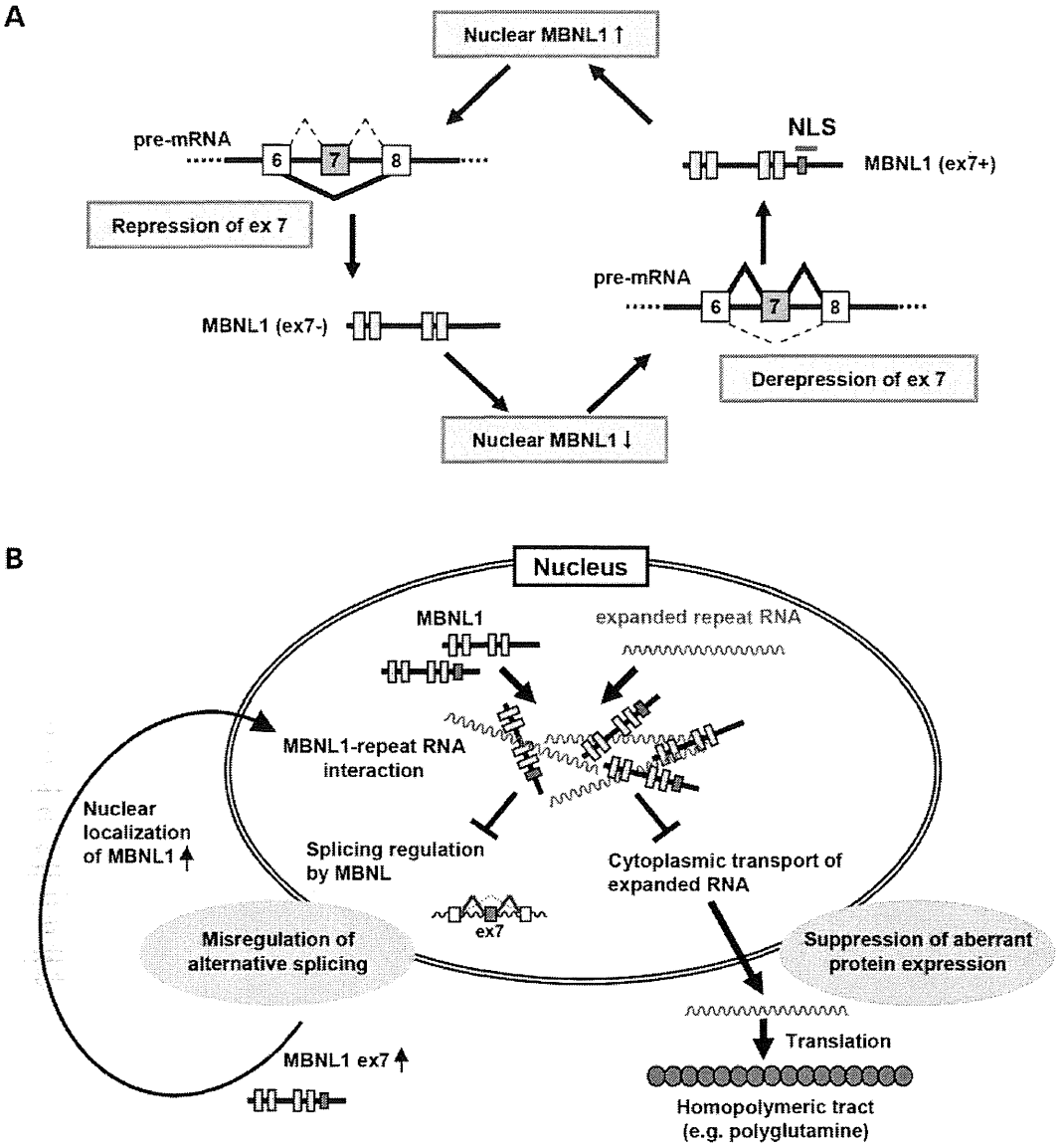

Figure 9. Autoregulation of MBNL1 and a novel aspect of MBNL–RNA interaction in the nucleus. (**A**) Autoregulation of MBNL1. Nuclear MBNL function can be maintained through feedback autoregulation. Increased activity of MBNL proteins in the nucleus leads to exon 7 skipping, which results in the production of MBNL1 isoforms lacking an NLS. This may in turn lead to reduced MBNL activity in the nucleus, resulting in an increase in exon 7 inclusion. Such a feedback mechanism may limit the amount of nuclear MBNL proteins. (**B**) In the presence of expanded-repeat RNA as in disease conditions, the activity of MBNL proteins is reduced, leading to enhanced exon 7 inclusion. This in turn leads to accumulation of MBNL1-containing NLS in the nucleus and may enhance interaction with expanded-repeat RNA. The interaction of MBNL1 and repeat RNA also causes nuclear retention of the repeat RNA, which prevents the expression of aberrant homopolymeric proteins such as polyQ.

results are consistent with the notion that repeat-MBNL interaction induces RNA foci formation that have two consequences, reduced MBNL activities and suppression of repeat-derived proteins (Fig. 9B). In HD mice and StHdh cells, this interaction was somehow inefficient, possibly because (i) expanded CAG repeat binds to MBNL proteins less strongly than CUG repeat, (ii) the length of CAG repeat was relatively short, (iii) the level of endogenous MBNL proteins or mutant RNA was not sufficient and/or (iv) some co-factor or modifications of Mbnl proteins were lacked in the brain of HD mice and/or StHdh cells. However, in all cell types we have tested, overexpression of $MBNL1_{42}$ induced RNA foci formation, suggesting that a certain level of nuclear MBNL proteins can overcome the limitations mentioned earlier. Our results would warrant further investigations of HD mouse models based on the overexpression of MBNL proteins.

MBNL proteins might provide a basis for the development of therapies to reduce aberrant protein expression associated with repeat expansion. For example, compounds that mimic MBNL1 and induce nuclear retention of mutant transcripts would prevent toxic effects of homopolymeric proteins (45). Another therapeutic implication is that MBNL-mediated

nuclear RNA retention would facilitate selective degradation of mutant RNA, as RNA in the nucleus is susceptible to antisense oligonucleotide-mediated degradation (46).

Recently, dipeptide repeat proteins were found in C9-ALS/FTD that is caused by a hexanucleotide repeat expansion (47–52). In addition, polyglycine-containing protein was found in fragile X-associated tremor/ataxia syndrome (FXTAS) (50). These repetitive proteins are generated from non-coding tracts through RAN translation. The pronounced expression of expanded-repeat-derived proteins in HD, C9-ALS/FTD and FXTAS indicates that nuclear retention of expanded RNA might be inefficient in the cells of these diseases. Remarkably, the distributions of RNA foci and dipeptide repeat inclusions were largely segregated in the brain regions of C9-ALS/FTD (52), consistent with our model of reciprocal relationship between RNA foci formation and RAN translation (Fig. 9B) and its dependence on cell types. Owing to RAN translation, all transcribed repeat tracts may potentially have both RNA and protein toxicities (21). The relative contribution of these toxicities in each disease would be an important future subject. Our results suggest the importance of RNA-binding proteins as key factors involved in both RNA- and protein-mediated pathogenesis of repeat expansion diseases.

MATERIALS AND METHODS

cDNA clones and constructs

cDNA of human MBNL1, MBNL2 and MBNL3 were described previously (37). To facilitate mutagenesis, a silent mutation of L281L (c843t), which eliminates a XhoI site, was introduced into MBNL1 cDNA and the mutant was designated MBNL1/L281L. For making MBNL1 deletion, L281L was used as a PCR template together with a BamHI-added forward primer and an XhoI-added reverse primer. The amplified fragments were digested with BamHI and XhoI and then inserted in the BglII-SalI sites of pEGFP-C1 (Clontech). N-terminus regions of Mbnl1, Mbnl2 and Mbnl3 were described previously (37). Constructs encoding an *Actn1* minigene and RFP-Bimax2 were described previously (35,37). A DMPK3′-N3 construct with CTG18, interrupted CTG480, interrupted CTG900 or interrupted CAG480 contained two terminal exons as well as the intervening intron of human *DMPK* gene, which were excised from RFP-DMPK3′ constructs (37) and inserted into pCMV-N3, a tag-less vector made by deleting the EGFP fragment from pEGFP-N3 (Clontech). The *Mbnl1* minigene fragment covering exon 6 to exon 8 was amplified from mouse genomic DNA by PCR using a primer set of BamHI-Mbnl1-ex6-Fw and SalI-Mbnl1-ex8-Rv, in which restriction sites for BamHI and SalI were added, respectively. These fragments were cleaved by BglII and the SalI and then subcloned into the BglII-SalI restriction sites of pEGFP-C1. Non-coding CAG or CTG repeat constructs were made by inserting interrupted repeat fragments into the XhoI site of pcDNA3.1 V5-His A, B or C (Invitrogen). Constructs for microRNA-based RNAi were described previously (37). miMbnl1-236 and miMbnl2-675 were used for knockdown of murine endogenous Mbnl1 and Mbnl2, respectively. For simultaneous knockdown of Mbnl1 and Mbnl2, miMbnl1-146 was utilized (37).

Cell culture and transfection

COS-7 and N2a cells were maintained in Dulbecco's modified Eagle's medium and 10% fetal bovine serum. For minigene assays, cells were typically cultured in 12-well plates and transfected with 0.5 μg of plasmids for protein expression (or cognate empty vector) and 10 or 20 ng of plasmids for the expression of a minigene using Lipofectamine 2000 (Invitrogen) according to the manufacturer's instructions. When multiple plasmids were transfected for protein expression, the total amount of plasmids was adjusted to 0.5 μg. For microscopic studies, cells were plated in 8-well chamber slides and transfected with 120 ng of plasmids in total. For subcellular localization studies, cells were plated in a 24-well or 96-well plate. The cell line expressing EGFP-MBNL1$_{40}$ (A6) was described previously (37). The following cell lines were obtained from the NIGMS Human Genetic Cell Repository at the Coriell Institute for Medical Research (GM04647:DM1000 and GM04795:control). StHdh cells were obtained from Dr Macdonald and CHDI through Coriell Institute. These cell lines were maintained as recommended by the supplier. We used FuGENE HD (Promega) diluted in OPTI-MEM (Invitrogen) for transfection of StHdh cells.

Cellular splicing assay

Cellular splicing assay was performed as previously described (37). For *Mbnl1* splicing, minigene fragments were amplified by PCR using a fluorescein isothiocyanate (FITC)-labeled forward primer for a 3′ region of EGFP sequence, FITC-GFP-Fw, and a gene-specific reverse primer, Mbnl1-splicing-Rv2. PCR products were resolved by 2.0–2.5% agarose gel electrophoresis. The fluorescence of PCR products was captured and visualized by LAS-1000 (FUJIFILM) or ImageQuant LAS 4000 (GE Healthcare Japan). Intensity of band signals was analyzed using Multigauge software (FUJIFILM).

Quantitative PCR

Gene-specific primers were designed using Primer Express software (Applied BioSystems) and are listed in Supplementary Material, Table S1. cDNA and gene-specific primer sets were mixed with Power SYBR Green PCR Master Mix (Applied BioSystems) or Fast Start Universal SYBR Green Master (Roche). Real-time amplification and quantification were performed using ABI7700 (Applied BioSystems) or LightCycler 480 II (Roche) following the manufacturer's protocol.

Fluorescence *in situ* hybridization

Fluorescence in situ hybridization was performed essentially as previously described with minor modifications (6,53). Cells plated in the 8-well chamber slides or 96-well plates were transfected using Lipofectamine 2000 (Invitrogen). Twenty-four hours post-transfection, cells were fixed with 4% paraformaldehyde–PBS for 0.5–1 h. Cells were treated for 5 min with 2% acetone–PBS pre-chilled at −30°C for permeabilization, followed by 10 min of pre-hybridization using 40% formamide–2× SSC solution. When necessary, DNase or RNase was treated before pre-hybridization. Hybridization mixture

contained 40% formamide, 2 × SSC, vanadyl-nucleoside complex, BSA, yeast tRNA and 1 ng/ml (CTG)8 or (CAG)8 probe conjugated with Alexa-647 or -546. We also used Cy3-conjugated 2-O-methyl-modified RNA (CUG)8 or (CAG)8 probes at the same concentration. Hybridization was performed at 37°C for 2–3 h. After hybridization, cells were washed with 40% formamide–2 × SSC and PBS. Cells were treated with Hoechst33342 (300 mg/ml) in PBS for 40 min to stain the nuclei followed by PBS wash three times. VECTASHIELD Mounting Medium (Vector Laboratories, Inc.) was used for mounting. Fluorescent images were obtained by sequential scan using a Leica TCS SP2 MP confocal microscope. 40 × and 63 × objectives were used. Obtained images were processed using Adobe Photoshop 5.5.

Subcellular localization analysis

Cells were plated on a 24-well or 96-well plate. Typically at 24 h after transfection, cells were fixed by 4% PFA–PBS containing Hoechst33342 for 0.5–1 h at room temperature followed by washing with PBS three times. In the case of repeat RNA localization analysis, FISH was performed using oligonucleotides labeled with Alexa-647, Alexa-546 or Cy3 (Supplementary Material, Table S1). Quantitative localization analysis was performed using ArrayScanVTI High Content Screening Reader (Cellomics) as previously described (35). An NCI was defined as (cytoplasmic intensity per pixel)/(cytoplasmic intensity per pixel + nuclear intensity per pixel). In one experiment, at least 150 cells were analyzed for each construct and the average NCI value of the cell population was calculated.

SUPPLEMENTARY MATERIAL

Supplementary Material is available at *HMG* online.

ACKNOWLEDGEMENTS

We thank Dr M. MacDonald and CHDI for StHdh cells and Ms Tomoko Yoda and Ms Itsuko Yamamoto for animal maintenance and the staff members of Research Resource Center at RIKEN Brain Science Institute for DNA sequencing and cell sorting. Y.K. was supported by the RIKEN Special Postdoctoral Researchers Program.

Conflict of Interest statement. None declared.

FUNDING

This work was supported by the Grant-in-Aid from the Ministry of Education, Culture, Sports, Science, and Technology of Japan to N.N. (22110004, 22240037, 24659436 and 25253066) and to Y.K. (19790620, 21790854, 23791007 and 25461299) and by a Grant-in-Aid for the Research on Measures for Ataxic Diseases from the Ministry of Health, Welfare and Labor to N.N.

REFERENCES

1. La Spada, A.R. and Taylor, J.P. (2010) Repeat expansion disease: progress and puzzles in disease pathogenesis. *Nat. Rev. Genet.*, **11**, 247–258.
2. DeJesus-Hernandez, M., Mackenzie, I.R., Boeve, B.F., Boxer, A.L., Baker, M., Rutherford, N.J., Nicholson, A.M., Finch, N.A., Flynn, H., Adamson, J. *et al.* (2011) Expanded GGGGCC hexanucleotide repeat in noncoding region of C9ORF72 causes chromosome 9p-linked FTD and ALS. *Neuron*, **72**, 245–256.
3. Kobayashi, H., Abe, K., Matsuura, T., Ikeda, Y., Hitomi, T., Akechi, Y., Habu, T., Liu, W., Okuda, H. and Koizumi, A. (2011) Expansion of intronic GGCCTG hexanucleotide repeat in NOP56 causes SCA36, a type of spinocerebellar ataxia accompanied by motor neuron involvement. *Am. J. Hum. Genet.*, **89**, 121–130.
4. Renton, A.E., Majounie, E., Waite, A., Simon-Sanchez, J., Rollinson, S., Gibbs, J.R., Schymick, J.C., Laaksovirta, H., van Swieten, J.C., Myllykangas, L. *et al.* (2011) A hexanucleotide repeat expansion in C9ORF72 is the cause of chromosome 9p21-linked ALS-FTD. *Neuron*, **72**, 257–268.
5. Liquori, C.L., Ricker, K., Moseley, M.L., Jacobsen, J.F., Kress, W., Naylor, S.L., Day, J.W. and Ranum, L.P. (2001) Myotonic dystrophy type 2 caused by a CCTG expansion in intron 1 of ZNF9. *Science*, **293**, 864–867.
6. Mankodi, A., Urbinati, C.R., Yuan, Q.P., Moxley, R.T., Sansone, V., Krym, M., Henderson, D., Schalling, M., Swanson, M.S. and Thornton, C.A. (2001) Muscleblind localizes to nuclear foci of aberrant RNA in myotonic dystrophy types 1 and 2. *Hum. Mol. Genet.*, **10**, 2165–2170.
7. Rudnicki, D.D., Holmes, S.E., Lin, M.W., Thornton, C.A., Ross, C.A. and Margolis, R.L. (2007) Huntington's disease-like 2 is associated with CUG repeat-containing RNA foci. *Ann. Neurol.*, **61**, 272–282.
8. Daughters, R.S., Tuttle, D.L., Gao, W., Ikeda, Y., Moseley, M.L., Ebner, T.J., Swanson, M.S. and Ranum, L.P. (2009) RNA gain-of-function in spinocerebellar ataxia type 8. *PLoS Genet.*, **5**, e1000600.
9. Kino, Y., Mori, D., Oma, Y., Takeshita, Y., Sasagawa, N. and Ishiura, S. (2004) Muscleblind protein, MBNL1/EXP, binds specifically to CHHG repeats. *Hum. Mol. Genet.*, **13**, 495–507.
10. Jiang, H., Mankodi, A., Swanson, M.S., Moxley, R.T. and Thornton, C.A. (2004) Myotonic dystrophy type 1 is associated with nuclear foci of mutant RNA, sequestration of muscleblind proteins and deregulated alternative splicing in neurons. *Hum. Mol. Genet.*, **13**, 3079–3088.
11. Lin, X., Miller, J.W., Mankodi, A., Kanadia, R.N., Yuan, Y., Moxley, R.T., Swanson, M.S. and Thornton, C.A. (2006) Failure of MBNL1-dependent post-natal splicing transitions in myotonic dystrophy. *Hum. Mol. Genet.*, **15**, 2087–2097.
12. Fardaei, M., Rogers, M.T., Thorpe, H.M., Larkin, K., Hamshere, M.G., Harper, P.S. and Brook, J.D. (2002) Three proteins, MBNL, MBLL and MBXL, co-localize in vivo with nuclear foci of expanded-repeat transcripts in DM1 and DM2 cells. *Hum. Mol. Genet.*, **11**, 805–814.
13. Kanadia, R.N., Johnstone, K.A., Mankodi, A., Lungu, C., Thornton, C.A., Esson, D., Timmers, A.M., Hauswirth, W.W. and Swanson, M.S. (2003) A muscleblind knockout model for myotonic dystrophy. *Science*, **302**, 1978–1980.
14. Kanadia, R.N., Shin, J., Yuan, Y., Beattie, S.G., Wheeler, T.M., Thornton, C.A. and Swanson, M.S. (2006) Reversal of RNA missplicing and myotonia after muscleblind overexpression in a mouse poly(CUG) model for myotonic dystrophy. *Proc. Natl. Acad. Sci. USA*, **103**, 11748–11753.
15. Chamberlain, C.M. and Ranum, L.P. (2012) Mouse model of muscleblind-like 1 overexpression: skeletal muscle effects and therapeutic promise. *Hum. Mol. Genet.*, **21**, 4645–4654.
16. Hao, M., Akrami, K., Wei, K., De Diego, C., Che, N., Ku, J.H., Tidball, J., Graves, M.C., Shieh, P.B. and Chen, F. (2008) Muscleblind-like 2 (Mbnl2)-deficient mice as a model for myotonic dystrophy. *Dev. Dyn.*, **237**, 403–410.
17. Charizanis, K., Lee, K.Y., Batra, R., Goodwin, M., Zhang, C., Yuan, Y., Shiue, L., Cline, M., Scotti, M.M., Xia, G. *et al.* (2012) Muscleblind-like 2-mediated alternative splicing in the developing brain and dysregulation in myotonic dystrophy. *Neuron*, **75**, 437–450.
18. Bauer, P.O. and Nukina, N. (2009) The pathogenic mechanisms of polyglutamine diseases and current therapeutic strategies. *J. Neurochem.*, **110**, 1737–1765.
19. Moseley, M.L., Zu, T., Ikeda, Y., Gao, W., Mosemiller, A.K., Daughters, R.S., Chen, G., Weatherspoon, M.R., Clark, H.B., Ebner, T.J. *et al.* (2006) Bidirectional expression of CUG and CAG expansion transcripts and intranuclear polyglutamine inclusions in spinocerebellar ataxia type 8. *Nat. Genet.*, **38**, 758–769.
20. Wilburn, B., Rudnicki, D.D., Zhao, J., Weitz, T.M., Cheng, Y., Gu, X., Greiner, E., Park, C.S., Wang, N., Sopher, B.L. *et al.* (2011) An antisense

CAG repeat transcript at JPH3 locus mediates expanded polyglutamine protein toxicity in Huntington's disease-like 2 mice. *Neuron*, **70**, 427–440.
21. Zu, T., Gibbens, B., Doty, N.S., Gomes-Pereira, M., Huguet, A., Stone, M.D., Margolis, J., Peterson, M., Markowski, T.W., Ingram, M.A. *et al.* (2011) Non-ATG-initiated translation directed by microsatellite expansions. *Proc. Natl. Acad. Sci. USA*, **108**, 260–265.
22. Li, L.B., Yu, Z., Teng, X. and Bonini, N.M. (2008) RNA toxicity is a component of ataxin-3 degeneration in Drosophila. *Nature*, **453**, 1107–1111.
23. Hsu, R.J., Hsiao, K.M., Lin, M.J., Li, C.Y., Wang, L.C., Chen, L.K. and Pan, H. (2011) Long tract of untranslated CAG repeats is deleterious in transgenic mice. *PLoS One*, **6**, e16417.
24. Mykowska, A., Sobczak, K., Wojciechowska, M., Kozlowski, P. and Krzyzosiak, W.J. (2011) CAG repeats mimic CUG repeats in the misregulation of alternative splicing. *Nucl. Acids Res.*, **39**, 8938–8951.
25. Wang, L.C., Chen, K.Y., Pan, H., Wu, C.C., Chen, P.H., Liao, Y.T., Li, C., Huang, M.L. and Hsiao, K.M. (2011) Muscleblind participates in RNA toxicity of expanded CAG and CUG repeats in *Caenorhabditis elegans*. *Cell Mol. Life Sci.*, **68**, 1255–1267.
26. Ho, T.H., Savkur, R.S., Poulos, M.G., Mancini, M.A., Swanson, M.S. and Cooper, T.A. (2005) Colocalization of muscleblind with RNA foci is separable from mis-regulation of alternative splicing in myotonic dystrophy. *J. Cell Sci.*, **118**, 2923–2933.
27. Yuan, Y., Compton, S.A., Sobczak, K., Stenberg, M.G., Thornton, C.A., Griffith, J.D. and Swanson, M.S. (2007) Muscleblind-like 1 interacts with RNA hairpins in splicing target and pathogenic RNAs. *Nucl. Acids Res.*, **35**, 5474–5486.
28. Dhaenens, C.M., Schraen-Maschke, S., Tran, H., Vingtdeux, V., Ghanem, D., Leroy, O., Delplanque, J., Vanbrussel, E., Delacourte, A., Vermersch, P. *et al.* (2008) Overexpression of MBNL1 fetal isoforms and modified splicing of Tau in the DM1 brain: two individual consequences of CUG trinucleotide repeats. *Exp. Neurol.*, **210**, 467–478.
29. Gates, D.P., Coonrod, L.A. and Berglund, J.A. (2011) Autoregulated splicing of muscleblind-like 1 (MBNL1) Pre-mRNA. *J. Biol. Chem.*, **286**, 34224–34233.
30. Fernandez-Costa, J.M. and Artero, R. (2010) A conserved motif controls nuclear localization of *Drosophila Muscleblind*. *Mol. Cells*, **30**, 65–70.
31. Tran, H., Gourrier, N., Lemercier-Neuillet, C., Dhaenens, C.M., Vautrin, A., Fernandez-Gomez, F.J., Arandel, L., Carpentier, C., Obriot, H., Eddarkaoui, S. *et al.* (2011) Analysis of exonic regions involved in nuclear localization, splicing activity, and dimerization of Muscleblind-like-1 isoforms. *J. Biol. Chem.*, **286**, 16435–16446.
32. Dansithong, W., Paul, S., Comai, L. and Reddy, S. (2005) MBNL1 is the primary determinant of focus formation and aberrant insulin receptor splicing in DM1. *J. Biol. Chem.*, **280**, 5773–5780.
33. Smith, K.P., Byron, M., Johnson, C., Xing, Y. and Lawrence, J.B. (2007) Defining early steps in mRNA transport: mutant mRNA in myotonic dystrophy type I is blocked at entry into SC-35 domains. *J. Cell Biol.*, **178**, 951–964.
34. Querido, E., Gallardo, F., Beaudoin, M., Menard, C. and Chartrand, P. (2011) Stochastic and reversible aggregation of mRNA with expanded CUG-triplet repeats. *J. Cell Sci.*, **124**, 1703–1714.
35. Kino, Y., Washizu, C., Aquilanti, E., Okuno, M., Kurosawa, M., Yamada, M., Doi, H. and Nukina, N. (2011) Intracellular localization and splicing regulation of FUS/TLS are variably affected by amyotrophic lateral sclerosis-linked mutations. *Nucl. Acids Res.*, **39**, 2781–2798.
36. Gromak, N., Matlin, A.J., Cooper, T.A. and Smith, C.W. (2003) Antagonistic regulation of alpha-actinin alternative splicing by CELF proteins and polypyrimidine tract binding protein. *RNA*, **9**, 443–456.
37. Kino, Y., Washizu, C., Oma, Y., Onishi, H., Nezu, Y., Sasagawa, N., Nukina, N. and Ishiura, S. (2009) MBNL and CELF proteins regulate alternative splicing of the skeletal muscle chloride channel CLCN1. *Nucl. Acids Res.*, **37**, 6477–6490.
38. Kosugi, S., Hasebe, M., Entani, T., Takayama, S., Tomita, M. and Yanagawa, H. (2008) Design of peptide inhibitors for the importin alpha/beta nuclear import pathway by activity-based profiling. *Chem. Biol.*, **15**, 940–949.
39. Chook, Y.M. and Suel, K.E. (2011) Nuclear import by karyopherin-betas: recognition and inhibition. *Biochim. Biophys. Acta.*, **1813**, 1593–1606.
40. Terenzi, F. and Ladd, A.N. (2010) Conserved developmental alternative splicing of muscleblind-like (MBNL) transcripts regulates MBNL localization and activity. *RNA Biol.*, **7**, 43–55.
41. Lee, K.Y., Li, M., Manchanda, M., Batra, R., Charizanis, K., Mohan, A., Warren, S.A., Chamberlain, C.M., Finn, D., Hong, H. *et al.* (2013) Compound loss of muscleblind-like function in myotonic dystrophy. *EMBO Mol. Med.*, **5**, 1887–1900.
42. Adereth, Y., Dammai, V., Kose, N., Li, R. and Hsu, T. (2005) RNA-dependent integrin alpha3 protein localization regulated by the Muscleblind-like protein MLP1. *Nat. Cell Biol.*, **7**, 1240–1247.
43. Wang, E.T., Cody, N.A., Jog, S., Biancolella, M., Wang, T.T., Treacy, D.J., Luo, S., Schroth, G.P., Housman, D.E., Reddy, S. *et al.* (2012) Transcriptome-wide regulation of pre-mRNA splicing and mRNA localization by muscleblind proteins. *Cell*, **150**, 710–724.
44. de Mezer, M., Wojciechowska, M., Napierala, M., Sobczak, K. and Krzyzosiak, W.J. (2011) Mutant CAG repeats of Huntingtin transcript fold into hairpins, form nuclear foci and are targets for RNA interference. *Nucl. Acids Res.*, **39**, 3852–3863.
45. Oma, Y., Kino, Y., Sasagawa, N. and Ishiura, S. (2005) Comparative analysis of the cytotoxicity of homopolymeric amino acids. *Biochim. Biophys. Acta.*, **1748**, 174–179.
46. Wheeler, T.M., Leger, A.J., Pandey, S.K., MacLeod, A.R., Nakamori, M., Cheng, S.H., Wentworth, B.M., Bennett, C.F. and Thornton, C.A. (2012) Targeting nuclear RNA for in vivo correction of myotonic dystrophy. *Nature*, **488**, 111–115.
47. Ash, P.E., Bieniek, K.F., Gendron, T.F., Caulfield, T., Lin, W.L., Dejesus-Hernandez, M., van Blitterswijk, M.M., Jansen-West, K., Paul, J.W. 3rd, Rademakers, R. *et al.* (2013) Unconventional translation of C9ORF72 GGGGCC expansion generates insoluble polypeptides specific to c9FTD/ALS. *Neuron*, **77**, 639–646.
48. Mori, K., Arzberger, T., Grasser, F.A., Gijselinck, I., May, S., Rentzsch, K., Weng, S.M., Schludi, M.H., van der Zee, J., Cruts, M. *et al.* (2013) Bidirectional transcripts of the expanded C9orf72 hexanucleotide repeat are translated into aggregating dipeptide repeat proteins. *Acta. Neuropathol.*, **126**, 881–893.
49. Mori, K., Weng, S.M., Arzberger, T., May, S., Rentzsch, K., Kremmer, E., Schmid, B., Kretzschmar, H.A., Cruts, M., Van Broeckhoven, C. *et al.* (2013) The C9orf72 GGGGCC repeat is translated into aggregating dipeptide-repeat proteins in FTLD/ALS. *Science*, **339**, 1335–1338.
50. Todd, P.K., Oh, S.Y., Krans, A., He, F., Sellier, C., Frazer, M., Renoux, A.J., Chen, K.C., Scaglione, K.M., Basrur, V. *et al.* (2013) CGG repeat-associated translation mediates neurodegeneration in fragile X tremor ataxia syndrome. *Neuron*, **78**, 440–455.
51. Zu, T., Liu, Y., Banez-Coronel, M., Reid, T., Pletnikova, O., Lewis, J., Miller, T.M., Harms, M.B., Falchook, A.E., Subramony, S.H. *et al.* (2013) RAN proteins and RNA foci from antisense transcripts in C9ORF72 ALS and frontotemporal dementia. *Proc. Natl. Acad. Sci. USA*, **110**, E4968–E4977.
52. Gendron, T.F., Bieniek, K.F., Zhang, Y.J., Jansen-West, K., Ash, P.E., Caulfield, T., Daughrity, L., Dunmore, J.H., Castanedes-Casey, M., Chew, J. *et al.* (2013) Antisense transcripts of the expanded C9ORF72 hexanucleotide repeat form nuclear RNA foci and undergo repeat-associated non-ATG translation in c9FTD/ALS. *Acta Neuropathol.*, **126**, 829–844.
53. Fardaei, M., Larkin, K., Brook, J.D. and Hamshere, M.G. (2001) In vivo co-localisation of MBNL protein with DMPK expanded-repeat transcripts. *Nucl. Acids Res.*, **29**, 2766–2771.

The American Journal of Pathology, Vol. 184, No. 6, June 2014

ELSEVIER

The American Journal of
PATHOLOGY

ajp.amjpathol.org

ANIMAL MODELS

Laminin α1 Regulates Age-Related Mesangial Cell Proliferation and Mesangial Matrix Accumulation through the TGF-β Pathway

Liang Ning,* Hidetake Kurihara,† Susana de Vega,* Naoki Ichikawa-Tomikawa,*‡ Zhuo Xu,* Risa Nonaka,* Saiko Kazuno,§ Yoshihiko Yamada,¶ Jeffrey H. Miner,‖ and Eri Arikawa-Hirasawa*,**

From the Research Institute for Diseases of Old Age, the Departments of Anatomy and Life Structure† and Neurology,** and the Division of Proteomics and Biomolecular Science,§ the BioMedical Research Center, Juntendo University Graduate School of Medicine, Tokyo, Japan; the Department of Basic Pathology,‡ Fukushima Medical University School of Medicine, Fukushima, Japan; the National Institute of Dental and Craniofacial Research,¶ National Institutes of Health, Bethesda, Maryland; and the Renal Division,‖ Department of Internal Medicine, Washington University School of Medicine, St. Louis, Missouri

Accepted for publication February 18, 2014.

Address correspondence to Eri Arikawa-Hirasawa, M.D., Ph.D., Research Institute for Diseases of Old Age, Juntendo University Graduate School of Medicine, 2-1-1, Hongo, Bunkyo-ku, Tokyo 113-8421, Japan. E-mail: ehirasaw@juntendo.ac.jp.

Laminin α1 (LAMA1), a subunit of the laminin-111 basement membrane component, has been implicated in various biological functions *in vivo* and *in vitro*. Although LAMA1 is present in kidney, its roles in the kidney are unknown because of early embryonic lethality. Herein, we used a viable conditional knockout mouse model with a deletion of *Lama1* in the epiblast lineage ($Lama1^{CKO}$) to study the role of LAMA1 in kidney development and function. Adult $Lama1^{CKO}$ mice developed focal glomerulosclerosis and proteinuria with age. In addition, mesangial cell proliferation was increased, and the mesangial matrix, which normally contains laminin-111, was greatly expanded. *In vitro*, mesangial cells from $Lama1^{CKO}$ mice exhibited significantly increased proliferation compared with those from controls. This increased proliferation was inhibited by the addition of exogenous LAMA1-containing laminin-111, but not by laminin-211 or laminin-511, suggesting a specific role for LAMA1 in regulating mesangial cell behavior. Moreover, the absence of LAMA1 increased transforming growth factor (TGF)-β1–induced Smad2 phosphorylation, and inhibitors of TGF-β1 receptor I kinase blocked Smad2 phosphorylation in both control and $Lama1^{CKO}$ mesangial cells, indicating that the increased Smad2 phosphorylation occurred in the absence of LAMA1 via the TGF-β1 receptor. These findings suggest that LAMA1 plays a critical role in kidney function and kidney aging by regulating the mesangial cell population and mesangial matrix deposition through TGF-β/Smad signaling. *(Am J Pathol 2014, 184: 1683–1694; http://dx.doi.org/10.1016/j.ajpath.2014.02.006)*

Laminins comprise a family of heterotrimeric extracellular matrix (ECM) proteins consisting of α, β, and γ chains[1,2] that regulate cell attachment, proliferation, and differentiation.[3,4] During early embryogenesis, laminin α1 (LAMA1) first appears at the 16-cell stage and is later present in the two basement membranes (BMs) formed before gastrulation, the embryonic BM, and Reichert's membrane. In the developing kidney, temporal changes in laminin isoform expression occur as formation of glomeruli, the filtering unit of the kidney, proceeds. The earliest precursor of the glomerular BM (GBM) contains laminin-111 (LM-111; α1β1γ1). In contrast, the GBM contains LM-521 (α5β2γ1) at later developmental stages and in adulthood. Although LAMA1 is absent from the mature GBM, it is present in the glomerular mesangial matrix, an amorphous matrix made by mesangial cells that is one of the few prominent sites in which laminins are present outside of a definitive BM.[5] The glomerular capillary wall consists of podocytes with

Supported by a Ministry of Education, Culture, Sports, Science, and Technology (MEXT), Japan, Grant-in-Aid for Young Scientists (B) 24790860 (L.N.) and grants 17082008 and 2230023 (E.A.-H.), NIH Intramural Program of the National Institute of Dental and Craniofacial Research grant (Y.Y.), NIH grant R01DK078314 (J.H.M.), and MEXT–Supported Program for the Strategic Research Foundation at Private Universities (2011 to 2015).

Disclosures: None declared.

http://dx.doi.org/10.1016/j.ajpath.2014.02.006

interdigitated foot processes bridged by slit diaphragms, glomerular endothelial cells, and the intervening GBM[6] that these two cell types together produce.[7] Mesangial cells (MCs), the third cell type of the glomerulus, comprise approximately one-third of the glomerular tuft cell population. MCs bind the GBM at the base of the glomerular capillary loops to establish and maintain the structural architecture of the glomerular capillaries,[6] similar to the function of certain microvascular pericytes. These cells also contribute to mesangial matrix homeostasis, regulate filtration surface area and capillary blood pressure, and phagocytose apoptotic cells and immune complexes formed at or delivered to the glomerular capillaries. Cell biological and biochemical studies have characterized MC responses to hormones, cytokines, growth factors, and metabolic, inflammatory, and immune mediators that are highly relevant to primary glomerular diseases or to systemic diseases that target glomerular cells.[8]

Because inactivation of the *Lama1* gene in mice results in a failure of assembly of Reichert's membrane and developmental arrest shortly after implantation,[9] *in vivo* studies of LAMA1 function have been limited. Herein, we used a conditional *Lama1* knockout (KO) mouse model ($Lama1^{CKO}$) with specific deletion of *Lama1* in the epiblast lineage using *Sox2-Cre* to study the role of LAMA1 in kidney development and function. We found that the absence of LAMA1 delayed glomerular development, and adult $Lama1^{CKO}$ mice developed focal glomerulosclerosis and proteinuria with age. MCs from $Lama1^{CKO}$ mice showed increased proliferation, resulting in expansion of the mesangial cell compartment. Thus, LAMA1 plays a critical role in MC homeostasis and kidney function.

Materials and Methods

Animal Experiments

Conventional *Lama1* KO ($Lama1^{del/del}$) mice die at approximately embryonic day 7 because of lack of Reichert's membrane.[9,10] In a previous study, floxed *Lama1* ($Lama1^{flox/flox}$) mice and heterozygous *Lama1* null mice carrying the *Sox2-Cre* transgene ($Lama1^{del/+}$; $Sox2\text{-}Cre^{cre/+}$) were generated.[11] $Lama1^{CKO}$ ($Lama1^{floxed/del}$; $Sox2\text{-}Cre^{cre/+}$) mice with a conditional *Lama1* deficiency, specifically in the epiblast, and its derivatives, which comprise the entire embryo, were then generated by crossing the two lines. Genotypes were confirmed by PCR of tail-snip DNA.[11] Animals examined included male and female mice, aged 1 day to 24 months. $Lama1^{flox/flox}$ [wild-type (WT)] mice and $Lama1^{flox/del}$ (heterozygous) mice were used as normal controls.

Immunofluorescence

Kidneys from 7-month-old mice were fixed with 4% PFA in 0.1 mol/L PBS, pH 7.4, overnight at 4°C and then cryoprotected in 30% sucrose in PBS for 72 hours at 4°C. Sections (4 μm thick) were cut with a cryostat and mounted onto glass slides. For immunostaining, the frozen sections were air dried and washed with PBS. The sections were incubated with 0.1% Triton X-100 (Polysciences, Inc., Warrington, UK) in PBS for 15 minutes. After washing, they were blocked with blocking buffer (5% normal donkey serum and 2% bovine serum albumin in PBS) for 30 minutes and incubated with dilutions of the primary antibody in the blocking buffer for 1 hour. The following primary antibodies were used: rabbit anti-laminin α1 (LAMA1)[12]; rabbit anti-laminin α2 (LAMA2), rabbit anti-laminin α3 (LAMA3), rabbit anti-laminin α4 (LAMA4), and rabbit anti-laminin α5 (LAMA5) (gifts from Dr. Takako Sasaki); rat anti-laminin γ1 (LAMC1) (Chemicon International, Inc., Temecula, CA); mouse anti-synaptopodin (Progen Biotechnik, Heidelberg, Germany); rat anti-platelet endothelial cell adhesion molecule (PECAM; BD Pharmingen, Erembodegem, Belgium); and rabbit anti-smooth muscle actin (Abcam, Cambridge, MA). The slides were washed with PBS and incubated with the secondary antibodies, Alexa 488 donkey anti-rabbit (Molecular Probes, Eugene, OR), Cy3 donkey anti-mouse, and Cy 5–conjugated donkey anti-rat (Jackson ImmunoResearch Laboratories, Baltimore, MD) for 1 hour. In each experiment, several sections were incubated without the primary antibody to serve as controls. When the primary antibody was omitted from the staining, no immunoreactivity was observed.

Histological and Morphometric Data

For histological data, mice were perfused with 4% paraformaldehyde (PFA) under anesthesia. Kidney pieces from 2- to 24-month-old mice were fixed in 4% PFA and embedded in paraffin. Sections (4 μm thick) were deparaffinized with xylene, hydrated in a graded series of ethanol, and washed with PBS.

For morphometric analysis of glomeruli, sections were stained with either PAS or toluidine blue. Mesangial area was quantified by a blind observer (L.N.). Fifteen glomeruli cut at the vascular pole were randomly selected in PAS-stained sections from each animal in each experimental group. The increase in mesangial matrix (defined as mesangial area) was determined by the presence of PAS-positive and nuclei-free areas in the mesangium; the glomerular area was also traced along the outline of capillary loops using Imaging System KS400 (Imaging Associates, Thame, UK).

For electron microscopy, small pieces of kidney cortex from neonatal and 2- to 16-month-old mice were fixed in 2.5% glutaraldehyde in PBS. Tissues were dehydrated and embedded in plastic, and ultrathin sections were viewed by transmission electron microscopy, as previously described.[13] GBM thickness at 15 months of age in three $Lama1^{CKO}$ mice and three heterozygous mice was determined by using the orthogonal intercept method.[14] The degree of foot process effacement was evaluated by foot process width. A foot process was defined as any connected epithelial segment butting on the basement membrane between two neighboring filtration pores or slits. From each image, the

arithmetic mean of the foot process width was calculated, as described previously,[15] using the following equation:

$$\pi/4 \times \sum \text{GBM length} \Big/ \sum \text{foot process.} \quad (1)$$

where $\sum$ foot process is the total number of foot processes counted in each image, $\sum$ GBM length is the total GBM length measured in each image, and the correction factor of $\pi/4$ serves to correct for presumed random variation in the angle of section relative to the long axis of the podocyte.

Urine Albumin and Creatinine Assays

At monthly intervals beginning at 4 months of age, mice were placed in metabolic cages, and urine was collected for 24 hours. In some cases, 10 μL of urine in loading buffer was analyzed on SDS-PAGE gels stained with Coomassie Brilliant Blue. The urinary albumin-creatinine ratio was determined by immunoassay (DCA Vantage Analyzer; Siemens Healthcare Diagnostics, Deerfield, IL).

Cell Culture

Glomeruli were isolated through the injection of magnetic beads, which become trapped within glomerular capillaries.[16] Briefly, anesthetized 2-month-old mice were perfused with 8×10^7 Dynabeads M-450 (Invitrogen, Carlsbad, CA). The kidneys were removed and minced on ice, followed by digestion at 37°C with 1 mg/mL collagenase and 100 U/mL DNase I for 30 minutes, then filtered twice with 100-μm Falcon cell strainers (BD Falcon, Bedford, MA). The tissue was pelleted by gentle centrifugation (200 × *g*, 5 minutes), and glomeruli containing Dynabeads were collected using a magnetic particle concentrator (Dynal, Oslo, Norway) and washed in HBSS three times. Isolated glomeruli were cultured on type I collagen-coated culture dishes (BD BIOCOAT, Bedford, MA) in Dulbecco's modified Eagle's medium supplemented with 20% heat-inactivated fetal bovine serum, 100 μg/mL streptomycin, and 100 U/mL penicillin at 37°C in a humidified 95%/5% air/CO_2 atmosphere. When primary glomerular explant cultures reached day 30, cells were washed with PBS and removed from dishes by trypsinization (0.05% trypsin). Cells at passage 5 to 8 were characterized and used for the experiments. MCs cultured on chamber slides were fixed in 4% PFA and processed for immunofluorescence microscopy using antibodies for podocytes, endothelial cells, and MCs, as described previously.[17]

Analysis of Cell Proliferation

MCs were seeded in 8-well chamber slides (5×10^3 cells per well) and cultured with or without 5 μg/mL LM-111, LM-211, or LM-511 (Biolamina, Sundbyberg, Sweden). After 48 hours of culture, cell proliferation was assessed by measuring the incorporation of 5-bromo-2′-deoxyuridine (BrdU) into cellular DNA by an immunofluorescence assay (Kit 1-1296736; Roche, East Sussex, UK). Cells were incubated with 10 μmol/L BrdU (final concentration) for 60 minutes before fixation. The number of BrdU-positive cells was counted and expressed as a percentage of the total number of cells counted per field. At least five separate fields per well were examined. A negative control in which the anti-BrdU primary antibody was omitted was also assayed in each trial.

RT-PCR and Real-Time PCR Analysis

Total RNA was extracted from the MCs with TRIzol reagent, according to the manufacturer's instructions (Invitrogen). cDNA was synthesized from 2 μg of total RNA using oligo dT primers (Invitrogen) and Superscript III Reverse Transcriptase (Invitrogen). Real-time quantitative PCR (qPCR) was performed using SYBR Green PCR Master MIX and an ABI Prism 7500 Fast Sequence Detection System (Applied Biosystems, Santa Clara, CA). The primers used for transforming growth factor (TGF)-β1, glyceraldehyde-3-phosphate dehydrogenase (GAPDH) amplification were as follows: TGF-β1 5′-ACCTTGGTAACCGGCTGC-3′ (forward) and 5′-TCCTTGGTTCAGCCACTGC-3′ (reverse); and GAPDH 5′-ACGGCAAATTCAACGGCACAG-3′ (forward) and 5′-AGACTCCACGACATACTCAGCAC-3′ (reverse). Each sample was run in triplicate and normalized to GAPDH expression.

ELISA Data

A sample of 1 N HCl (20 μL) was added to 100 μL of cell culture supernatant and incubated for 10 minutes to activate latent TGF-β1. After the supernatants were neutralized with 1.2 N NaOH/0.5 mol/L HEPES, the samples were analyzed with a commercial TGF-β1 sandwich enzyme-linked immunosorbent assay (ELISA; R&D Systems, Minneapolis, MN), according to the manufacturer's recommendations. A standard curve was constructed using serial dilutions of ultrapure human TGF-β1 (R&D Systems). The amount of secreted TGF-β1 was normalized using total cellular proteins. Each sample was measured in duplicate.

Western Blot Analysis

MCs were seeded at a density of 3×10^5 cells per dish, grown to 70% confluence, and cultured in the absence or presence of 5 μg/mL LM-111 for 24 hours. After serum starvation for 24 hours in the absence or presence of 5 μg/mL LM-111, cells were treated with 10 ng/mL TGF-β1 (WAKO, Osaka, Japan) for 30 minutes. To study the effect of TGF-β1 receptor I (TβRI) kinase inhibitors on Smad2 phosphorylation, cells were serum starved and treated with increasing concentrations of SB-431542 (0.1, 1, 5, and 10 μmol/L) or dimethyl sulfoxide (Sigma-Aldrich, St. Louis, MO) in the presence of 10 ng/mL TGF-β1 for 30 minutes.[18] Protein extracts were prepared in lysis buffer (Cell Signaling, Danvers, MA) containing 1 mmol/L phenylmethylsulfonyl fluoride, 10 mmol/L

Na_3VO_4, and 2 mmol/L NaF, as well as phosphatase inhibitor cocktail. After incubation at 4°C for 30 minutes, nuclear and cellular debris were removed by centrifugation at 20,000 × *g* for 15 minutes at 4°C. Protein was quantified by BCA assay (Thermo Scientific, Rockford, IL) and 10 μg of protein per lane was separated by SDS-PAGE. Western blot analysis was performed as described previously.[19] The primary antibody used was anti–phospho-Smad2 (Ser465/467) (1:1000; Cell Signaling). The blots were subsequently reprobed with anti-Smad2/3 (1:1000; Cell Signaling). For the TβRI and collagen IV (COLIV) expression analysis, primary antibodies for TβRI (1:1000; Abcam) and COLIV (1:1000; Abcam) were used. The blots were subsequently reprobed with anti–β-actin antibody (1:1000; Santa Cruz Biotechnology, Inc., Santa Cruz, CA). Horseradish peroxidase–labeled secondary antibody to rabbit IgG or mouse IgG (1:1000) was purchased from GE Healthcare (Piscataway, NJ). Super Signal West Dura Extended Duration Substrate (Thermo Scientific) was used for detection of signals, and the images were captured using LAS-3000 mini (Fujifilm, Tokyo, Japan). Densitometry analysis of band intensity was performed using Multi Gauge version 3.0 (Fujifilm).

Transfection

FuGENE HD (Promega, Madison, WI) was used for transfection. Mesangial cells were plated on 6-well plates, grown to 50% to 60% confluence, and then transfected with either pcDNA3.1-*Lama1* or control pcDNA3.1. FuGENE HD Transfection Reagent (3 μL) was added to the DNA solution (1 μg in 100 μL Optimem). The mixture was incubated for 15 minutes at room temperature, then added to the cells. The cells were treated with TGF-β1 for 24 hours after transfection.

Statistical Analysis

Data are expressed as means ± SEM. A two-sided Student's *t*-test was used for comparisons between two groups. $P < 0.05$ was considered statistically significant.

Results

Delayed Kidney Development in Lama1-Deficient (*Lama1*^{CKO}) Mice

LAMA1 has been implicated in kidney development on the basis of results from organotypic cultures.[20,21] However, the *in vivo* function of LAMA1 in kidney is unknown, primarily because *Lama1* KO mice die at early embryonic stages. Herein, we used a viable conditional KO mouse (*Lama1*^{CKO}) model with a Sox2-Cre–mediated deletion of *Lama1* specifically in the epiblast lineage, which produces all embryonic tissues.[22] This enabled us to study the role of LAMA1 in kidney development and function. We first examined developing nephrons in newborn *Lama1*^{CKO} mice because all stages of nephrogenesis can be visualized in the newborn cortex.[22] We observed all appropriate developmental stages in both control and *Lama1*^{CKO} mice, including mesenchymal condensates and comma-shaped bodies (data not shown), S-shaped bodies (Figure 1, A and D), capillary loop stages with forming glomerular capillaries (Figure 1, B and E), and maturing glomeruli with blood cells in the capillaries (Figure 1, C and F). We next quantitated the extent of nephron/glomerular development for each developmental stage in control and *Lama1*^{CKO} mice as percentages of the total (Figure 1G). The percentage of maturing and fully mature glomeruli was significantly decreased in *Lama1*^{CKO} mice compared with controls. These results showed that glomerular development was delayed in *Lama1*^{CKO} mice. To investigate whether the delay in glomerular development caused fewer nephrons in *Lama1*^{CKO} mice, we measured numbers of glomeruli in *Lama1*^{CKO} and control kidneys from 2-month-old mice. We found that there was no significant difference in numbers of glomeruli between control and *Lama1*^{CKO} mice (Figure 1H).

Renal Abnormalities in Adult *Lama1*^{CKO} Mice

Laminin isoform composition differs in GBM and in the mesangial matrix, and it changes with glomerular development.[5,23] In some renal diseases, the normal transition and final composition are altered.[22,24–28] Immunostaining revealed that, in *Lama1*^{CKO} mice, LAMA1 was absent from the mesangium (Figure 2B), whereas it was expressed in control mice (Figure 2A), as shown previously.[5] LAMA2 was detected in the mesangium at a higher level in mutant versus control (Figure 2, C and D), and LAMA4 was also detected weakly in glomeruli of both control and *Lama1*^{CKO} mice (Figure 2, E and F). LAMA5 was detected in virtually all GBM segments (Figure 2, G and H), in agreement with previous studies.[5] LAMC1 (γ1) was detected in both the GBM and the mesangium in control and in *Lama1*^{CKO} kidneys, but increased in the *Lama1*^{CKO} mesangium (Figure 2, I and J). These data show that even though LAMA1 was absent from glomeruli, the distribution of the other laminin α chains in glomeruli was similar to those of normal mice, except for stronger immunostaining for LAMA2 and LAMC1 in the mesangium of *Lama1*^{CKO} mice.

Increased levels of LAMA2 and LAMC1 (as well as perlecan; data not shown) in the mesangium indicated a possible expansion of the mesangial compartment in *Lama1*^{CKO} kidneys. Histological examination by light microscopy revealed abnormalities in *Lama1*^{CKO} mice compared with the control exclusively in glomeruli. In agreement with the immunofluorescence, dividing kidneys into sections (9 heterozygous, 1 WT, and 11 *Lama1*^{CKO} females at 7 months), followed by PAS staining, showed mesangial expansion in *Lama1*^{CKO} mice (Figure 3, A–D). Mesangial expansion was quantitated by a morphometric analysis; the PAS-positive and nuclei-free mesangial area in the glomeruli of *Lama1*^{CKO} mice was 44% more than that in

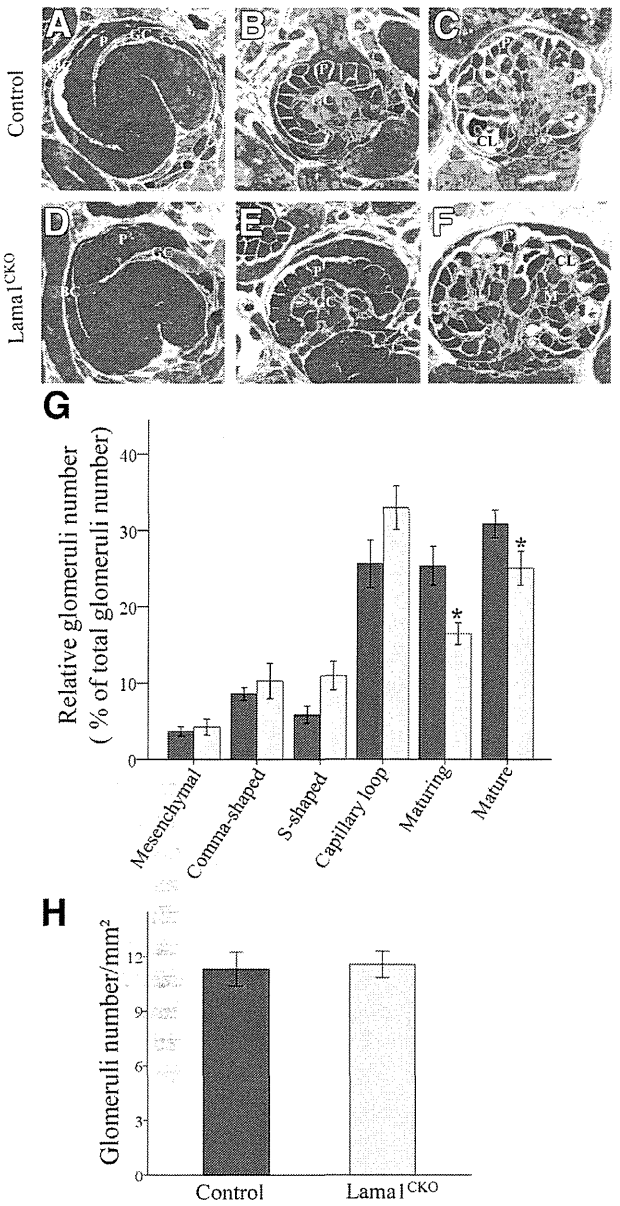

Figure 1 Histological characteristics of glomerular development. **A–F:** Toluidine blue–stained sections from newborn (post-natal day 1) mouse kidneys. **A** and **D:** S-shaped body. A capillary loop is present in the cleft. **B** and **E:** Capillary loop stage glomeruli showing the cup-shaped arrangement of the podocytes. **C** and **F:** Mature glomeruli. The percentage of glomeruli at each developmental stage in control and *Lama1*^{CKO} mice. **G:** Significantly lower percentages of maturing and mature glomeruli are observed in *Lama1*^{CKO} kidneys (light gray bars) compared with the controls (dark gray bars). **H:** There is no significant difference in the number of glomeruli observed in *Lama1*^{CKO} versus control kidneys at 2 months of age. Data represent means ± SEM. *$P < 0.05$ versus control at same glomerular developmental stage. Original magnification, ×1000 (**A–F**). BC, Bowman's capsule; CL, capillary loop; GC, glomerular cleft; M, mesangial cells; P, podocyte progenitors.

control mice (Figure 3E). Total glomerular area was defined by tracing along the outline of the capillary loops and was decreased in *Lama1*^{CKO} mice compared with control mice (Figure 3F). Thus, the relative mesangial area, as calculated by determining the mesangial area/total glomerular area ratio, was increased by 67% in the *Lama1*^{CKO} mice (Figure 3G).

Taken together, these findings indicate that LAMA1 plays a role in mesangial cell homeostasis and that other laminin α chains cannot substitute for Lama1 in mediating this function.

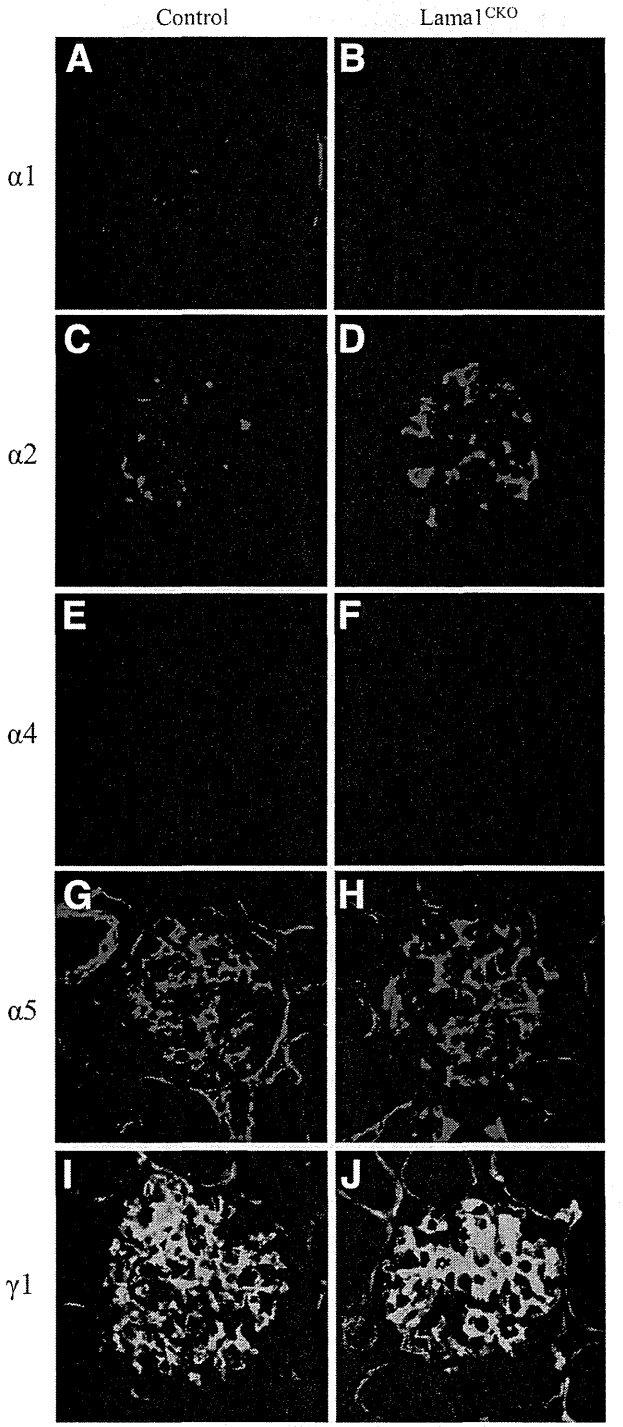

Figure 2 Immunofluorescence microscopic analysis of laminin chain deposition. Basement membranes and mesangial matrix were stained with anti-laminin α1, α2, α4, and α5 (red), and anti-laminin γ1 (green) antibodies, as indicated. LMα1 is detected in the mesangial matrix in control mice (**A**) and is absent in *Lama1*^{CKO} mice (**B**). There are no detectable differences in laminin α chain immunolocalization (**C–J**), but LMα2 and LMγ1 increase in the mesangial matrix in *Lama1*^{CKO} mice (**D** and **J**). Original magnification, ×400 (**A–J**).

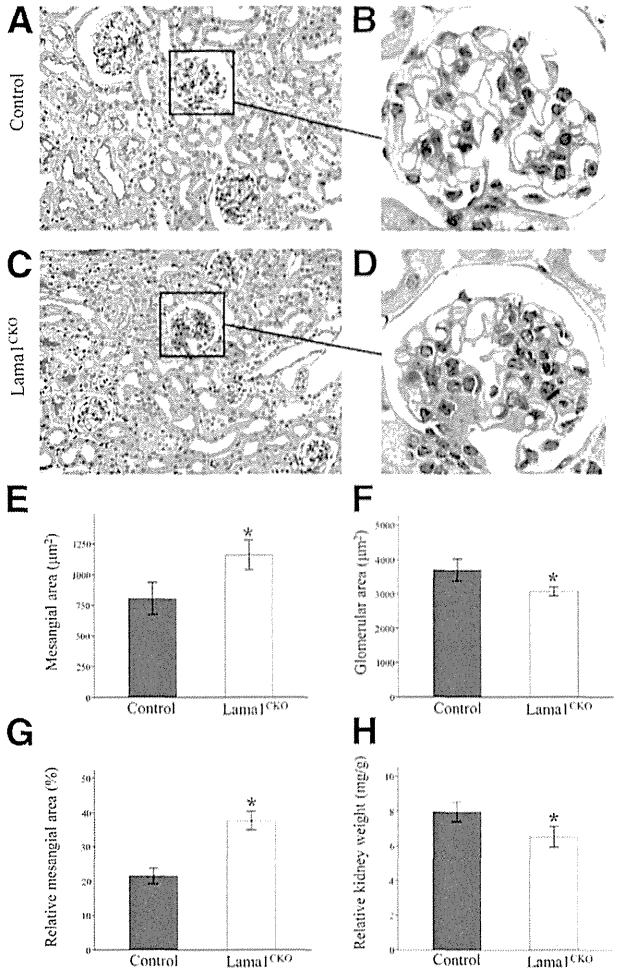

Figure 3 Light microscopy reveals renal abnormalities in adult *Lama1*^{CKO} mice. **A**—**D:** Representative images of PAS-stained kidney specimens from 6- to 8-month-old control and *Lama1*^{CKO} mice. **C** and **D:** Glomerular size reduction and mesangial expansion are observed in *Lama1*^{CKO} mice. The graphs depict quantitative measurements of mesangial area (**E**), glomerular area (**F**), and relative mesangial matrix area (**G**) of control (dark gray bars) versus *Lama1*^{CKO} (light gray bars) mice. **H:** The average kidney weight relative to total body weight is shown. Data represent means ± SEM. $^{*}P < 0.05$ versus control. Original magnifications: ×400 (**A** and **C**); ×1000 (**B** and **D**).

In addition to the abnormalities in the mesangium, a significant difference in kidney weight between *Lama1*^{CKO} mice and control mice was observed, with the kidney weight of *Lama1*^{CKO} mice being lower than that of controls at 7 months of age (data not shown). These differences remained significant when values were normalized to body weight (Figure 3H).

Lama1^{CKO} Mice Develop Glomerulosclerosis with Increased MC Proliferation and Mesangial Matrix Expansion with Age

We next examined aging-associated glomerular pathological features in *Lama1*^{CKO} mice at 2 to 24 months of age. Before 6 months of age, no significant renal histopathological changes were observed in either control or *Lama1*^{CKO} mice (data not shown). However, after 6 months of age, *Lama1*^{CKO} mice showed mesangial cell proliferation and mesangial matrix expansion compared with control mice (Figure 4, D—F and J—L). As *Lama1*^{CKO} mice aged further, mesangial cell numbers stayed the same, but mesangial matrix expansion increased (Figure 4, M and N). By 6 to 8 months of age, *Lama1*^{CKO} mice showed a moderate mesangial matrix

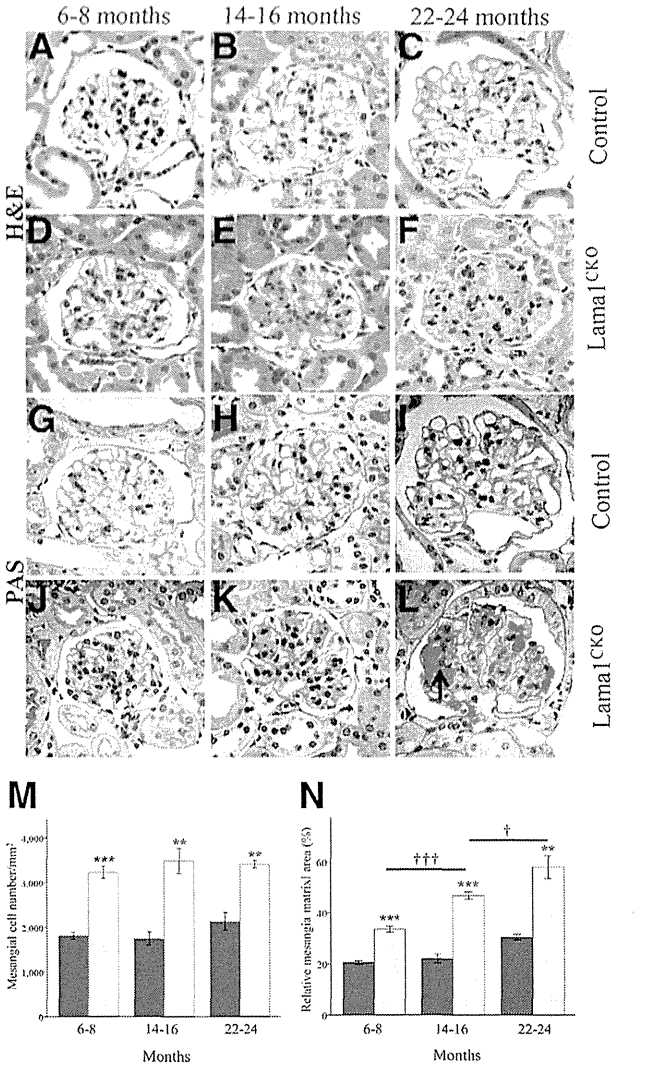

Figure 4 Light microscopy reveals progressive development of glomerulosclerosis in *Lama1*^{CKO} mice. Representative micrographs of PAS- and H&E-stained glomeruli in control and *Lama1*^{CKO} mice aged 7, 15, and 23 months (as indicated). H&E staining shows matrix expansion in the *Lama1*^{CKO} mouse (**D**—**F**) compared with the control (**A**—**C**). **E:** At 14 to 16 months, the *Lama1*^{CKO} mice showed moderate mesangial sclerosis. **F:** As the *Lama1*^{CKO} mice aged, mesangial sclerosis became more conspicuous. PAS staining revealed increased mesangial cell proliferation and GBM thickening in the *Lama1*^{CKO} (**J**—**L**) compared with the control (**G**—**I**) mice. **L:** PAS^{+} nodular mesangial sclerosis was observed in *Lama1*^{CKO} mice at 22 to 24 months of age (**arrow**). **M** and **N:** Quantitative measurements of mesangial cell number and relative mesangial matrix area (per total glomerular tuft cross-sectional area) for control (dark gray bars) and *Lama1*^{CKO} (light gray bars) mice. Data represent means ± SEM. $^{**}P < 0.01$, $^{***}P < 0.001$ versus control at same age; $^{\dagger}P < 0.05$ versus 14- to 16-month-old mice; $^{\dagger\dagger\dagger}P < 0.001$ versus 6- to 8-month-old mice. Original magnification, ×1000 (**A**—**L**).

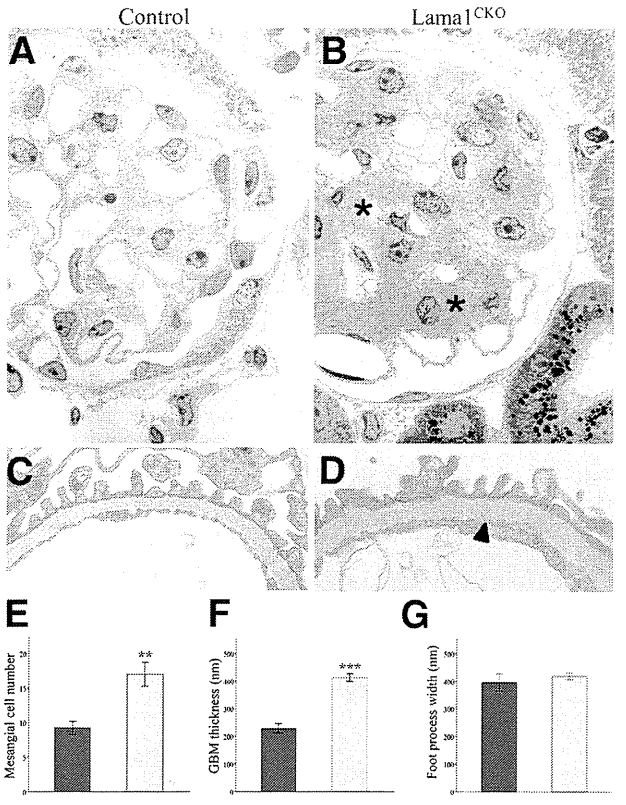

Figure 5 Electron microscopic analysis of glomeruli. Representative electron micrographs of control (**A** and **C**) and *Lama1*^{CKO} (**B** and **D**) glomeruli at 14 to 16 months of age. *Lama1*^{CKO} mice had significant mesangial expansion (**asterisks**) and GBM thickening (**arrowhead**). **E–G:** Quantitation of the indicated features in control (dark gray bars) and *Lama1*^{CKO} (light gray bars) mice show significant increases in mesangial cell number and GBM thickness but no significant difference was observed in podocyte foot process width. Data represent means ± SEM. $^{**}P < 0.01$, $^{***}P < 0.001$ versus control. Original magnifications: ×1000 (**A** and **B**); ×10,000 (**C** and **D**).

expansion, but they did not exhibit glomerulosclerosis (Figure 4, D and J). By 14 to 16 months of age, 35% of *Lama1*^{CKO} mice showed numerous segmentally sclerosed glomeruli (Figure 4E) associated with GBM thickening (Figure 4K), whereas no control mice showed glomerulosclerosis with GBM thickening (Figure 4, B and H). By 22 to 24 months of age, most Lama1^{CKO} mice had many globally and segmentally sclerosed glomeruli (Figure 4, F and L), and PAS^{+} nodular mesangial sclerosis was observed (Figure 4L). Control mice also showed moderate mesangial expansion and GBM thickening at this age, but only rarely showed glomerulosclerosis (Figure 4, C and I). Glomerular abnormalities were characterized in more detail by electron microscopy in mice aged 14 to 16 months (Figure 5). In agreement with light microscopy, there were more MCs and an increased amount of mesangial matrix in old *Lama1*^{CKO} mice compared with controls (Figure 5B). Many areas of GBM thickening were also observed (Figure 5D). These data show that older *Lama1*^{CKO} mice exhibit a greater degree of MC and matrix irregularities versus controls, presumably associated with aging.

Defects in Renal Function of *Lama1*^{CKO} Mice

Because glomerular structure can influence glomerular filtration,[6] the glomerular abnormalities in *Lama1*^{CKO} mice led us to look for alterations in renal function. Urine from *Lama1*^{CKO} and control mice was collected every 2 months and analyzed (Figure 6). Coomassie Blue staining of urine samples from *Lama1*^{CKO} mice showed an increased level of albumin compared with controls (Figure 6A). We also consistently detected higher urinary albumin/creatinine ratios in *Lama1*^{CKO} mice at 6 to 24 months of age, and the difference increased as the mice aged (Figure 6B). These results demonstrate a progressive defect in the kidney's ability to handle albumin in *Lama1*^{CKO} mice.

MCs from *Lama1*^{CKO} Mice Show Increased Proliferation *in Vitro*

In vivo studies have provided evidence that LAMA1 deficiency promotes MC proliferation. To investigate this further, we examined MC proliferation *in vitro*. Primary cultures derived from mouse glomeruli yielded a homogeneous population of MCs (Figure 7, A–C). These were characterized by their stellate/spindle-shaped morphological features, positive staining for α-smooth muscle actin, and negative staining for synaptopodin and PECAM, which are specific for podocytes and endothelial cells, respectively. MCs from *Lama1*^{CKO} mice exhibited significantly increased proliferation compared with those from control mice (Figure 7D).

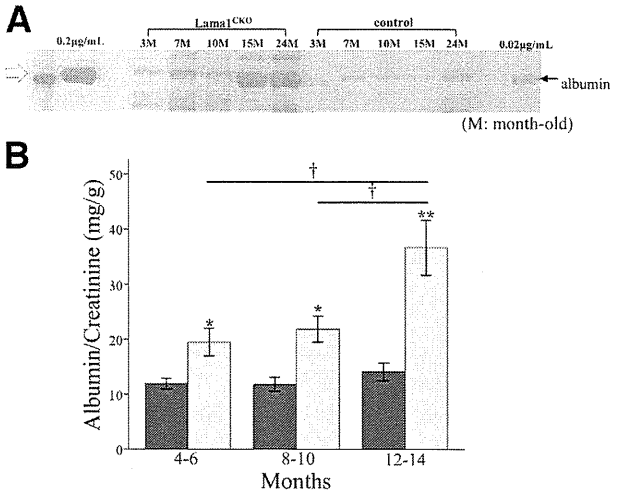

Figure 6 Analysis of renal function. **A:** Urine from 3- to 24-month-old (M) *Lama1*^{CKO} and control mice was collected and analyzed by SDS-PAGE and Coomassie Blue staining. The **arrow** denotes approximately 66 KDa, the size of excreted albumin. *Lama1*^{CKO} mice have a higher concentration of albumin as they age compared with control mice. **B:** Urine was collected for 24 hours from control (dark gray bars) and *Lama1*^{CKO} (light gray bars) mice and analyzed for albumin/creatinine ratio. Ratios in *Lama1*^{CKO} mice are higher than in controls. Data represent means ± SEM. $^{*}P < 0.05$, $^{**}P < 0.01$ versus control; $^{\dagger}P < 0.05$ versus 4- to 6-month-old mice and 8- to 10-month-old mice.

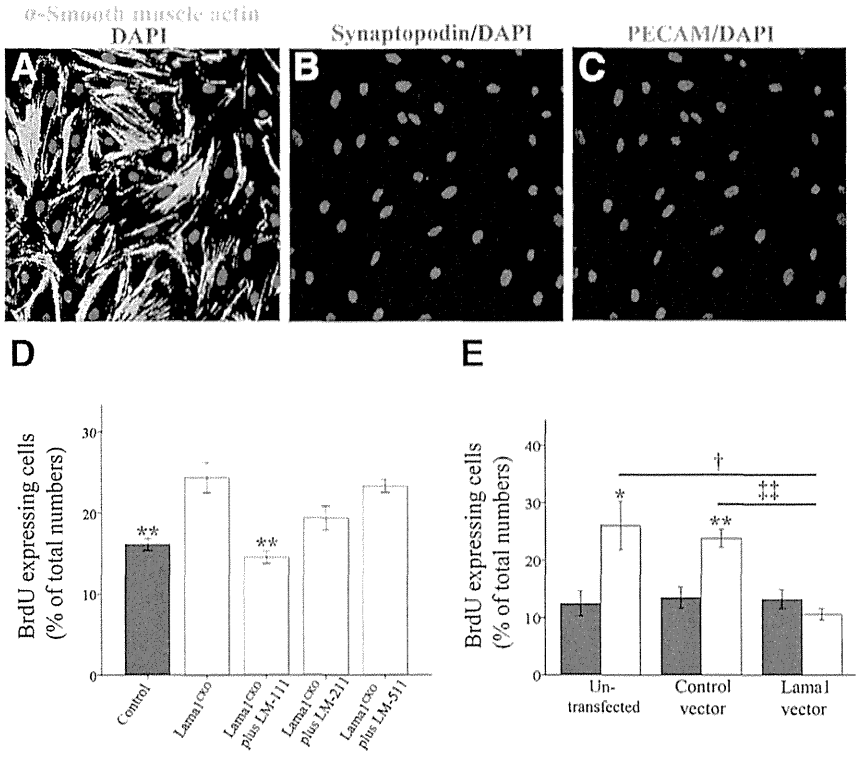

Figure 7 Analysis of primary mesangial cells. Mesangial cells are elongated, arranged in multiple layers, and stained positively for smooth muscle α-actin (**A**), but not synaptopodin (**B**) or PECAM (**C**). **D:** Proliferation was assessed by immunofluorescence assay for BrdU-positive cells as a percentage of the total number of cells, averaged from five separate fields of view. Mesangial cells from *Lama1*^{CKO} mice exhibit significantly increased proliferation compared with control cells. This increase is inhibited by exogenous LAMA1-containing LM-111, but not by LAMA2- or LAMA5-containing isoforms. **E:** Mesangial cell proliferation determined in cells transfected with vector alone or with a LAMA1 expression vector. Control (dark gray bars) and *Lama1*^{CKO} (light gray bars) cells were cultured on slide chambers for 24 hours and transfected for 48 hours before proliferation analysis. Restoration of LAMA1 expression by *Lama1*^{CKO} cells suppresses their proliferation. Data represent means ± SEM. $^{*}P < 0.05$, $^{**}P < 0.01$ versus control; $^{\dagger}P < 0.05$ versus untransfected cells; $^{\ddagger\ddagger}P < 0.01$ versus control vector transfected cells.

After this, we tested MC proliferation by treatment with LM-111, LM-211, or LM-511. The increase in MC proliferation was inhibited by exogenous LM-111, but not by either LM-211 or LM-511 (Figure 7D). We also tested whether LAMA1 deficiency is directly involved in this increased MC proliferation by transfection of *Lama1*^{CKO} MCs with a *Lama1* expression vector. RT-qPCR analysis showed the expression of *Lama1* mRNA in *Lama1*^{CKO} MCs transfected with the *Lama1* vector (Supplemental Figure S1B). We found that the expression of exogenous *Lama1* abrogated the increased proliferation of *Lama1*^{CKO} MCs, whereas the control empty vector did not (Figure 7E), suggesting that LAMA1/LM-111 plays a specific role in regulating MC homeostasis.

Loss of LAMA1 Increases TGF-β/Smad Signaling in *Lama1*^{CKO} MCs

TGF-β/Smad signaling is a major pathway involved in renal fibrosis.[29] Binding of TGF-β1 to TβRII activates TβRI kinase, which phosphorylates Smad2 and Smad3. The phosphorylated Smad2 (p-Smad2) and p-Smad3 then bind to Smad4 and form the Smad complex, which translocates into the nucleus and regulates target gene transcription.[29] Smad7 is an inhibitory Smad that blocks TGF-β–induced Smad-dependent fibrosis. Because TGF-β1 stimulates the synthesis and inhibits the degradation of extracellular matrix molecules,[30] and is associated with increased mesangial matrix in several glomerular diseases,[30–32] we investigated the effect of the absence of LAMA1 on TGF-β signaling. We first examined the level of TGF-β1 mRNA and protein secreted in *Lama1*^{CKO} MCs. We did not detect significant differences compared with control MCs (Figure 8, A–C), indicating that the absence of LAMA1 does not alter the levels of TGF-β1 expression. Next, we examined the levels of p-Smad2 in the absence of LAMA1. The addition of TGF-β1 increased p-Smad2 levels to a greater extent in *Lama1*^{CKO} cells than in control cells (Figure 8D), suggesting that the absence of LAMA1 increases TGF-β/Smad signaling. The basal phosphorylation level of Smad2 in *Lama1*^{CKO} MCs was higher than that in control MCs (Supplemental Figure S2) when cells were cultured without serum starvation. In addition, LM-111 treatment rescued the increased TGF-β1–induced Smad2 phosphorylation in *Lama1*^{CKO} cells, implying that LAMA1 likely plays a direct role in dampening the levels of TGF-β1–mediated Smad2 phosphorylation in MCs. Furthermore, we sought to elucidate the mechanism of increased Smad2 phosphorylation in the absence of LAMA1. MCs were pretreated with SB431542, a specific and potent inhibitor of TGF-β–induced phosphorylation of Smad2 by TβRI.[33] SB431542 was added to the control and *Lama1*^{CKO} cells at varying doses, and cells were treated for 30 minutes with TGF-β1. Cell lysates were collected and processed for Western blot analysis of p-Smad2 levels. Decreased or loss of Smad2 phosphorylation was observed in a dose-dependent manner for both control and *Lama1*^{CKO} cells (Figure 8E). These data show that all of the phosphorylation of Smad2 occurs via the activity of TβRI, regardless of the presence or absence of LAMA1. This indicates that LAMA1 plays a direct role in limiting TGF-β/Smad

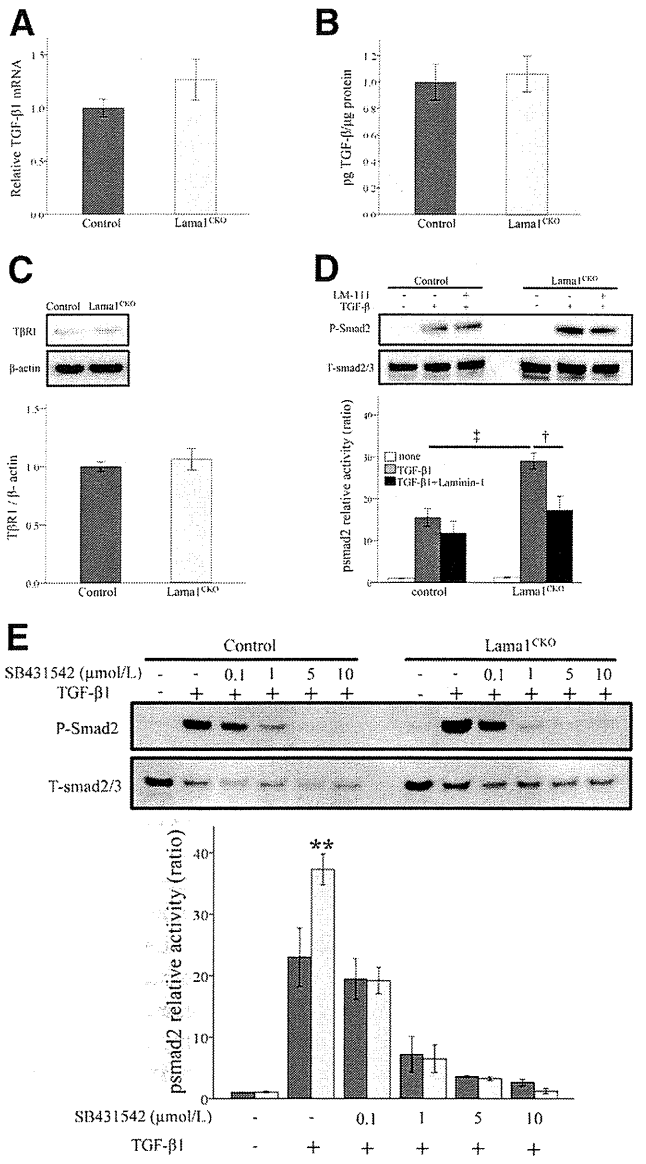

Figure 8 TGF-β1/Smad signaling in mesangial cells from *Lama1*^{CKO} and control mice. **A** and **B:** TGF-β1 mRNA expression and secretion in mesangial cells. MCs were cultured for 48 hours and serum starved for an additional 48 hours before total mRNA extraction and culture media collection. **A:** TGF-β1 mRNA expression levels measured by RT-qPCR. The bar graph represents the ratio between the TGF-β1 and GAPDH levels. **B:** Immunoreactive TGF-β1 synthesis measured by ELISA. **C:** Western blot analysis of TβRI protein levels in MCs. **D** and **E:** Smad2 phosphorylation determined by using Western blot analysis. The intensity of signal was analyzed by Multi Gauge version 3.0 (Fujifilm). Relative activity, expressed as the ratio of activated phospho-Smad2/total Smad2/3, was quantified as the fold increase relative to non-stimulation conditions (defined as 1). MCs from control and *Lama1*^{CKO} mice were cultured in the absence or presence of 5 μg/mL LM-111 for 24 hours. **D:** After serum starvation for 24 hours, cells were treated with 10 ng/mL TGF-β1 (WAKO) for 30 minutes. MCs from control and *Lama1*^{CKO} mice were serum starved for 24 hours, followed by 1-hour treatment with increasing concentrations of SB-431542 (0.1, 1, 5, and 10 μmol/L) or dimethyl sulfoxide (DMSO), and then stimulated for 30 minutes with 10 ng/mL TGF-β. **E:** Loss of Smad2 phosphorylation is observed in an SB-431542 dose-dependent manner for both control (dark gray bars) and *Lama1*^{CKO} (light gray bars) cells. Data represent means ± SEM. $^{**}P < 0.01$ versus control; $^{\dagger}P < 0.05$ versus laminin-1 treatment cells; $^{\ddagger}P < 0.01$ versus control cells.

signaling. Finally, because reduced Smad7 results in enhanced activation of TGF-β signaling,[34] we also investigated Smad7 expression in MCs. There was no significant difference in the level of Smad7 protein in control and in *Lama1*^{CKO} cells (data not shown).

TGF-β1–Induced Type IV Collagen Expression Is Increased in the Absence of LAMA1

Because *Lama1*^{CKO} mice showed a thickened GBM (Figure 5D), we examined the expression of COLIV, one of the major mesangial matrix components.[35] Immunostaining analysis revealed more COLIV deposition in the mesangium of *Lama1*^{CKO} mice than of control mice (Figure 9A). Previous studies have shown that TGF-β1 induces COLIV expression in mouse MCs.[36] Therefore, we examined the effect of TGF-β1 on COLIV expression in MCs prepared from *Lama1*^{CKO} mice. We found that TGF-β1 induced COLIV expression in both control and *Lama1*^{CKO} MCs, but the level of COLIV expression was significantly higher in *Lama1*^{CKO} MCs than in control cells (Figure 9, B and C). This higher COLIV expression level in *Lama1*^{CKO} MCs was abrogated by transfection with the LAMA1 expression vector, but not by transfection with the empty control vector (Figure 9D). These results suggest that LAMA1 is involved in the regulation of mesangial matrix production.

Discussion

Our interest in LM-111 function in the kidney was initially stimulated by the observation that *Lama1* has a rather restricted expression pattern. LAMA1 is found transiently in the developing GBM, is absent in the mature GBM, and is present in the glomerular mesangium in adult mice.[5] Herein, we demonstrated that Lama1 is critical for mesangial homeostasis and kidney function.

An impediment to elucidating kidney LAMA1 function had been that *Lama1* disruption results in lethality at an early embryonic stage.[1] We previously described the generation of a conditional KO of *Lama1* with selective deletion only in embryonic cells, wherein the early embryonic death observed in total *Lama1* KO mice was overcome. Our results demonstrate important functional roles for LAMA1, which are exemplified by delayed glomerular development, abnormal renal histological features, and impaired renal function. Increased MC proliferation and mesangial matrix expansion are remarkable features observed in *Lama1*^{CKO} mice.

Diabetic nephropathy is histologically characterized by thickening of the GBM and mesangial expansion.[37–39] The earliest morphological change in diabetic nephropathy is mesangial expansion due to increased mesangial matrix deposition and a mild increase in mesangial cellularity, as well as hypertrophy of mesangial cells. The characteristic histological changes of diabetic nephropathy are diffuse and

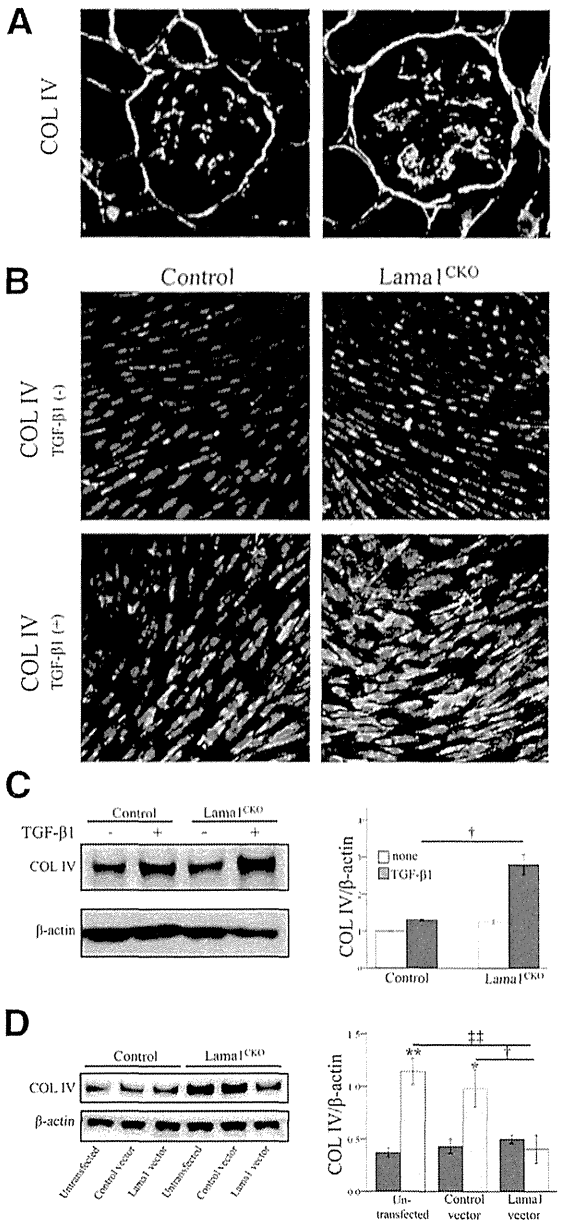

Figure 9 Expression of COLIV. **A:** The deposition of COLIV in the glomeruli of control and *Lama1*^{CKO} mice. Immunofluorescence staining for COLIV was performed in frozen tissue sections from 7-month-old mice. **B—D:** Effect of TGF-β1 on COLIV synthesis by MCs. Control and *Lama1*^{CKO} MCs were cultured on slide chambers for 24 hours, serum deprived for an additional 24 hours, and then treated with TGF-β1 for 24 hours. Immunofluorescence (**B**) and Western blot analysis (**C**) were performed to analyze COLIV synthesis and deposition. Values in **C** are expressed as COLIV/β-actin and quantified as the fold increase relative to control non-stimulation conditions (defined as 1). Control and *Lama1*^{CKO} MCs were cultured on 6-well plates for 24 hours and transfected for 48 hours before a 24-hour TGF-β1 treatment. $^{\dagger}P < 0.05$ versus TGF-β1 treatment control cells. **D:** COLIV protein levels were then determined by using Western blot analysis. β-Actin was used as a control. The intensity of signal was analyzed by Multi Gauge version 3.0 (Fujifilm). The absence of LAMA1 increases TGF-β1—induced COLIV expression. This increase was abrogated by transfection of *Lama1*^{CKO} (light gray bars) MCs with the LAMA1 expression vector; control MCs are represented by dark gray bars. $^{*}P < 0.05$, $^{**}P < 0.01$ versus control; $^{\dagger}P < 0.05$ versus control vector transfected cells; $^{\ddagger\ddagger}P < 0.01$ versus untransfected cells. Original magnification, ×400 (**A**).

nodular glomerulosclerosis, along with afferent and efferent hyaline arteriolosclerosis. A reduction in podocyte number is associated with foot process effacement.[40] In the present study, we observed GBM thickening, mesangial expansion, and increased mesangial cell proliferation from 6-month-old *Lama1*^{CKO} mice. As the mice aged, there was increased mesangial expansion due to glomerulosclerosis, which was accompanied by progressive proteinuria. These pathological conditions are similar to those seen in diabetic nephropathy, but we did not observe differences between *Lama1*^{CKO} and control mice in terms of podocyte number or foot process effacement. Although proteinuria was detectable in *Lama1*^{CKO} mice, this was at a lower level than in most kidney diseases. Because there is no or little LAMA1 in the GBM, podocytes would not be expected to have abnormalities. The proteinuria in the later stages was likely due to mesangial cell defects, which led to profibrotic cross talk that affected the podocytes, or perhaps due to some unknown mechanism.

Many studies have indicated that activated mesangial cells are the major cells responsible for the expression of interstitial matrix components, such as fibronectin and type I collagen, which directly result in mesangial expansion leading to glomerulosclerosis.[41] The present study demonstrated that the deletion of LAMA1 results in age-dependent mesangial expansion, which develops into focal glomerulosclerosis. These observations lead us to hypothesize that LAMA1 may be an endogenous negative regulator that specifically suppresses mesangial cell activation.

TGF-β is the most potent cytokine inducing mesangial cell activation both *in vitro* and *in vivo*.[42] It stimulates the expression of ECM proteins, including collagens, laminin, and fibronectin, while suppressing the synthesis of ECM protease inhibitors.[43] The Smad pathway is known to mediate the functions of TGF-β on renal fibrogenesis and subsequent ECM accumulation in diabetic nephropathy.[44] In the present study, we were unable to detect increased TGF-β1 mRNA expression in *Lama1*^{CKO} MCs. However, an alternative mechanism is suggested from the increased TGF-β1—induced Smad2 phosphorylation. In addition, inhibitors of TβRI kinase blocked Smad2 phosphorylation in both control and *Lama1*^{CKO} MCs. This supports the hypothesis that LAMA1 suppresses mesangial cell activation via inhibition of the TGF-β/Smad pathway.

Laminins not only function as structural components, but also bind cell surface receptors, including integrins and α-dystroglycan.[45] We demonstrated that LM-111 treatment abrogated the increased TGF-β1—induced Smad2 phosphorylation in *Lama1*^{CKO} cells. Furthermore, the restoration of LAMA1 expression in *Lama1*^{CKO} MCs by transfection with the LAMA1 expression vector inhibited the increased MC proliferation and TGF-β1—induced COLIV expression. We, therefore, speculate that LM-111 synthesized by WT mesangial cells inhibits TGF-β1 signaling. TGF-β1 signals through its type I and type II serine/threonine kinase receptors,[42] and this pathway is tightly controlled by multiple positive and negative regulator

proteins.[46] Negative regulation of TGF-β signaling is accomplished by the rapid attenuation or even inhibition of TβRI/II and/or Smad activities.[47,48] In extracellular compartments, decorin, a proteoglycan associated with matrix components, binds to active TGF-β1 and prevents it from engaging with its receptors.[49] In cell membranes, integrin signaling is involved in negatively regulating TGF-β signaling, because adhesion reduces TGF-β–induced Smad2 phosphorylation.[50] Laminins regulate cellular behavior through interactions with cell surface receptors, including integrins, syndecans, and α-dystroglycan.[1,51] In the cytoplasm, inhibitory Smad7 either competes with receptor-regulated Smad to bind to activated type I receptors or interacts with growth arrest and DNA damage protein, a regulatory subunit of the protein phosphatase 1 holoenzyme, which subsequently recruits catalytic subunit of PP1 to dephosphorylate and inactivate the TGF-β type I receptor.[52]

The present study demonstrated that excess Smad2 phosphorylation occurred in the absence of Lama1 via TβRI and the absence of LAMA1 did not change the expression of Smad7. In addition, the Biacore analysis and solid-phase binding assays showed that the active form of TGF-β bound to LM-111 (Supplemental Figure S3 and Supplemental Table S1). This suggests that LAMA1 may play a direct role in inhibiting TGF-β signaling by binding to active TGF-β1 to prevent it from engaging with its receptors or by interaction with integrin signaling, which is involved in negatively regulating TGF-β signaling.

Taken together, our results suggest that LAMA1 plays a role in negatively regulating TGF-β/Smad signaling. This may be important for maintaining mesangial cell populations and mesangial matrix deposition.

Acknowledgments

We thank Glenn Longenecker and Ashok B. Kulkarni for help generating mutant mice and Dr. Yasuo Uchiyama, Takashi Ueno, and Tsutomu Fujimura (Juntendo University, Tokyo, Japan) for useful advice.

Supplemental Data

Supplemental material for this article can be found at *http://dx.doi.org/10.1016/j.ajpath.2014.02.006*.

References

1. Miner JH, Yurchenco PD: Laminin functions in tissue morphogenesis. Annu Rev Cell Dev Biol 2004, 20:255–284
2. Aumailley M, Bruckner-Tuderman L, Carter WG, Deutzmann R, Edgar D, Ekblom P, Engel J, Engvall E, Hohenester E, Jones JC, Kleinman HK, Marinkovich MP, Martin GR, Mayer U, Meneguzzi G, Miner JH, Miyazaki K, Patarroyo M, Paulsson M, Quaranta V, Sanes JR, Sasaki T, Sekiguchi K, Sorokin LM, Talts JF, Tryggvason K, Uitto J, Virtanen I, von der Mark K, Wewer UM, Yamada Y, Yurchenco PD: A simplified laminin nomenclature. Matrix Biol 2005, 24:326–332
3. Ryan MC, Christiano AM, Engvall E, Wewer UM, Miner JH, Sanes JR, Burgeson RE: The functions of laminins: lessons from in vivo studies. Matrix Biol 1996, 15:369–381
4. Kleinman HK, Weeks BS, Schnaper HW, Kibbey MC, Yamamura K, Grant DS: The laminins: a family of basement membrane glycoproteins important in cell differentiation and tumor metastases. Vitam Horm 1993, 47:161–186
5. Miner JH, Patton BL, Lentz SI, Gilbert DJ, Snider WD, Jenkins NA, Copeland NG, Sanes JR: The laminin alpha chains: expression, developmental transitions, and chromosomal locations of alpha1-5, identification of heterotrimeric laminins 8-11, and cloning of a novel alpha3 isoform. J Cell Biol 1997, 137:685–701
6. Miner JH: Building the glomerulus: a matricentric view. J Am Soc Nephrol 2005, 16:857–861
7. Wang R, Moorer-Hickman D, St John PL, Abrahamson DR: Binding of injected laminin to developing kidney glomerular mesangial matrices and basement membranes in vivo. J Histochem Cytochem 1998, 46:291–300
8. Abboud HE: Mesangial cell biology. Exp Cell Res 2012, 318:979–985
9. Miner JH, Li C, Mudd JL, Go G, Sutherland AE: Compositional and structural requirements for laminin and basement membranes during mouse embryo implantation and gastrulation. Development 2004, 131:2247–2256
10. Alpy F, Jivkov I, Sorokin L, Klein A, Arnold C, Huss Y, Kedinger M, Simon-Assmann P, Lefebvre O: Generation of a conditionally null allele of the laminin alpha1 gene. Genesis 2005, 43:59–70
11. Ichikawa-Tomikawa N, Ogawa J, Douet V, Xu Z, Kamikubo Y, Sakurai T, Kohsaka S, Chiba H, Hattori N, Yamada Y, Arikawa-Hirasawa E: Laminin alpha1 is essential for mouse cerebellar development. Matrix Biol 2012, 31:17–28
12. Sasaki T: Expression and distribution of laminin α1 and α2 chains in embryonic and adult mouse tissues: an immunochemical approach. Exp Cell Res 2002, 275:185–199
13. Jarad G, Cunningham J, Shaw AS, Miner JH: Proteinuria precedes podocyte abnormalities in Lamb2-/- mice, implicating the glomerular basement membrane as an albumin barrier. J Clin Invest 2006, 116:2272–2279
14. Jensen EB, Gundersen HJ, Osterby R: Determination of membrane thickness distribution from orthogonal intercepts. J Microsc 1979, 115:19–33
15. Koop K, Eikmans M, Baelde HJ, Kawachi H, De Heer E, Paul LC, Bruijn JA: Expression of podocyte-associated molecules in acquired human kidney diseases. J Am Soc Nephrol 2003, 14:2063–2071
16. Takemoto M, Asker N, Gerhardt H, Lundkvist A, Johansson BR, Saito Y, Betsholtz C: A new method for large scale isolation of kidney glomeruli from mice. Am J Pathol 2002, 161:799–805
17. Yaoita E, Kurihara H, Sakai T, Ohshiro K, Yamamoto T: Phenotypic modulation of parietal epithelial cells of Bowman's capsule in culture. Cell Tissue Res 2001, 304:339–349
18. Nyati S, Schinske K, Ray D, Nyati MK, Ross BD, Rehemtulla A: Molecular imaging of TGFbeta-induced Smad2/3 phosphorylation reveals a role for receptor tyrosine kinases in modulating TGFbeta signaling. Clin Cancer Res 2011, 17:7424–7439
19. Hammerschmidt E, Loeffler I, Wolf G: Morg1 heterozygous mice are protected from acute renal ischemia-reperfusion injury. Am J Physiol Renal Physiol 2009, 297:F1273–F1287
20. Klein G, Langegger M, Timpl R, Ekblom P: Role of laminin A chain in the development of epithelial cell polarity. Cell 1988, 55:331–341
21. Sorokin LM, Conzelmann S, Ekblom P, Battaglia C, Aumailley M, Timpl R: Monoclonal antibodies against laminin A chain fragment E3 and their effects on binding to cells and proteoglycan and on kidney development. Exp Cell Res 1992, 201:137–144
22. Abrahamson DR, St John PL: Loss of laminin epitopes during glomerular basement membrane assembly in developing mouse kidneys. J Histochem Cytochem 1992, 40:1943–1953

23. Miner JH: Developmental biology of glomerular basement membrane components. Curr Opin Nephrol Hypertens 1998, 7:13–19
24. Peutz-Kootstra CJ, Hansen K, De Heer L, Abrass CK, Bruijn JA: Differential expression of laminin chains and anti-laminin autoantibodies in experimental lupus nephritis. J Pathol 2000, 192: 404–412
25. Abrahamson DR, Prettyman AC, Robert B, St John PL: Laminin-1 reexpression in Alport mouse glomerular basement membranes. Kidney Int 2003, 63:826–834
26. St John PL, Wang R, Yin Y, Miner JH, Robert B, Abrahamson DR: Glomerular laminin isoform transitions: errors in metanephric culture are corrected by grafting. Am J Physiol Renal Physiol 2001, 280: F695–F705
27. Kashtan CE, Kim Y, Lees GE, Thorner PS, Virtanen I, Miner JH: Abnormal glomerular basement membrane laminins in murine, canine and human Alport syndrome: aberrant laminin alpha2 deposition is species-independent. J Am Soc Nephrol 2001, 12:252–260
28. Cosgrove D, Rodgers K, Meehan D, Miller C, Bovard K, Gilroy A, Gardner H, Kotelianski V, Gotwals P, Amatucci A, Kalluri R: Integrin alpha1beta1 and transforming growth factor-beta1 play distinct roles in Alport glomerular pathogenesis and serve as dual targets for metabolic therapy. Am J Pathol 2000, 157: 1649–1659
29. Lan HY, Chung AC: TGF-beta/Smad signaling in kidney disease. Semin Nephrol 2012, 32:236–243
30. Ziyadeh FN: Different roles for TGF-beta and VEGF in the pathogenesis of the cardinal features of diabetic nephropathy. Diabetes Res Clin Pract 2008, 82(Suppl 1):S38–S41
31. Ziyadeh FN, Sharma K, Ericksen M, Wolf G: Stimulation of collagen gene expression and protein synthesis in murine mesangial cells by high glucose is mediated by autocrine activation of transforming growth factor-beta. J Clin Invest 1994, 93:536–542
32. Yoshioka K, Takemura T, Murakami K, Okada M, Hino S, Miyamoto H, Maki S: Transforming growth factor-beta protein and mRNA in glomeruli in normal and diseased human kidneys. Lab Invest 1993, 68:154–163
33. Inman GJ, Nicolas FJ, Callahan JF, Harling JD, Gaster LM, Reith AD, Laping NJ, Hill CS: SB-431542 is a potent and specific inhibitor of transforming growth factor-beta superfamily type I activin receptor-like kinase (ALK) receptors ALK4, ALK5, and ALK7. Mol Pharmacol 2002, 62:65–74
34. Heldin CH, Miyazono K, ten Dijke P: TGF-beta signalling from cell membrane to nucleus through SMAD proteins. Nature 1997, 390: 465–471
35. Kikkawa R, Togawa M, Isono M, Isshiki K, Haneda M: Mechanism of the progression of diabetic nephropathy to renal failure. Kidney Int Suppl 1997, 62:S39–S40
36. Chai Q, Krag S, Miner JH, Nyengaard JR, Chai S, Wogensen L: TGF-beta1 induces aberrant laminin chain and collagen type IV isotype expression in the glomerular basement membrane. Nephron Exp Nephrol 2003, 94:e123–e136
37. Falk RJ, Scheinman JI, Mauer SM, Michael AF: Polyantigenic expansion of basement membrane constituents in diabetic nephropathy. Diabetes 1983, 32(Suppl 2):34–39
38. Adler S: Structure-function relationships associated with extracellular matrix alterations in diabetic glomerulopathy. J Am Soc Nephrol 1994, 5:1165–1172
39. Mauer SM, Steffes MW, Ellis EN, Sutherland DE, Brown DM, Goetz FC: Structural-functional relationships in diabetic nephropathy. J Clin Invest 1984, 74:1143–1155
40. Alsaad KO, Herzenberg AM: Distinguishing diabetic nephropathy from other causes of glomerulosclerosis: an update. J Clin Pathol 2007, 60:18–26
41. Mason RM, Wahab NA: Extracellular matrix metabolism in diabetic nephropathy. J Am Soc Nephrol 2003, 14:1358–1373
42. Dai C, Liu Y: Hepatocyte growth factor antagonizes the profibrotic action of TGF-beta1 in mesangial cells by stabilizing Smad transcriptional corepressor TGIF. J Am Soc Nephrol 2004, 15:1402–1412
43. Schnaper HW, Kopp JB, Poncelet AC, Hubchak SC, Stetler-Stevenson WG, Klotman PE, Kleinman HK: Increased expression of extracellular matrix proteins and decreased expression of matrix proteases after serial passage of glomerular mesangial cells. J Cell Sci 1996, 109(Pt 10):2521–2528
44. Schnaper HW, Hayashida T, Poncelet AC: It's a Smad world: regulation of TGF-beta signaling in the kidney. J Am Soc Nephrol 2002, 13:1126–1128
45. Higaki Y, Schullery D, Kawata Y, Shnyreva M, Abrass C, Bomsztyk K: Synergistic activation of the rat laminin gamma1 chain promoter by the gut-enriched Kruppel-like factor (GKLF/KLF4) and Sp1. Nucleic Acids Res 2002, 30:2270–2279
46. ten Dijke P, Miyazono K, Heldin CH: Signaling inputs converge on nuclear effectors in TGF-beta signaling. Trends Biochem Sci 2000, 25:64–70
47. Di Guglielmo GM, Le Roy C, Goodfellow AF, Wrana JL: Distinct endocytic pathways regulate TGF-beta receptor signalling and turnover. Nat Cell Biol 2003, 5:410–421
48. Feng XH, Derynck R: Specificity and versatility in tgf-beta signaling through Smads. Annu Rev Cell Dev Biol 2005, 21:659–693
49. Border WA, Noble NA, Yamamoto T, Harper JR, Yamaguchi Y, Pierschbacher MD, Ruoslahti E: Natural inhibitor of transforming growth factor-beta protects against scarring in experimental kidney disease. Nature 1992, 360:361–364
50. Thannickal VJ, Lee DY, White ES, Cui Z, Larios JM, Chacon R, Horowitz JC, Day RM, Thomas PE: Myofibroblast differentiation by transforming growth factor-beta1 is dependent on cell adhesion and integrin signaling via focal adhesion kinase. J Biol Chem 2003, 278: 12384–12389
51. Gullberg D, Ekblom P: Extracellular matrix and its receptors during development. Int J Dev Biol 1995, 39:845–854
52. Shi W, Sun C, He B, Xiong W, Shi X, Yao D, Cao X: GADD34-PP1c recruited by Smad7 dephosphorylates TGFbeta type I receptor. J Cell Biol 2004, 164:291–300

Physiological Reports

Open Access

Physiological Reports ISSN 2051-817X

ORIGINAL RESEARCH

Perlecan deficiency causes endothelial dysfunction by reducing the expression of endothelial nitric oxide synthase

Risa Nonaka[1], Takafumi Iesaki[2], Susana de Vega[1], Hiroyuki Daida[3], Takao Okada[2], Takako Sasaki[4] & Eri Arikawa-Hirasawa[1]

1 Research Institute for Disease of Old Age, Juntendo University Graduate School of Medicine, Tokyo, Japan
2 Department of Physiology, Juntendo University Graduate School of Medicine, Tokyo, Japan
3 Department of Cardiovascular Medicine, Juntendo University Graduate School of Medicine, Tokyo, Japan
4 Department of Biochemistry, Faculty of Medicine, Oita University, Oita, Japan

Keywords
Endothelial cell, nitric oxide synthase, perlecan.

Correspondence
Eri Arikawa-Hirasawa, Juntendo University Graduate School of Medicine, Research Institute for Diseases of Old Age, 2-1-1 Hongo, Bunkyo-ku, Tokyo 113-8421, Japan.
Tel: +81-3-3814-3016
Fax: +81-3-3814-3016
E-mail: ehirasaw@juntendo.ac.jp

Funding Information
This work was supported by a Grant-in-Aid for Young Scientists (B) (24790783) to R.N. and a Grants-in-Aids from the Ministry of Education, Culture, Sports, Science and Technology as well as the Ministry of Health, Labor and Welfare of Japan, Grant for Neurological and Psychiatric Disorders of NCNP (26-8) to E A-H. This study was supported by Grants from MEXT-Supported Program for the Strategic Research Foundation at Private Universities (2011–2015).

Received: 8 October 2014; Revised: 16 December 2014; Accepted: 17 December 2014

doi: 10.14814/phy2.12272

Physiol Rep, 3 (1), 2015, e12272, doi: 10.14814/phy2.12272

Risa Nonaka and Takafumi Iesaki have contributed equally to this work.

Abstract

Perlecan is a major heparan sulfate proteoglycan found in the subendothelial extracellular matrix of the vascular wall. The aim of this study was to investigate the role of perlecan in the regulation of vascular tone. A previously developed conditional perlecan-deficient mouse model was used to measure changes in the isometric force of isolated aortic rings. The vessels were first precontracted with phenylephrine, and then treated with increasing concentrations of vasorelaxants. Endothelium-dependent relaxation, elicited by acetylcholine, was significantly reduced in the perlecan-deficient aortas, whereas endothelium-independent relaxation caused by the exogenous nitric oxide donor sodium nitroprusside remained well preserved. The expression of the endothelial nitric oxide synthase (eNOS) gene, detected by real-time polymerase chain reaction, was significantly decreased in the perlecan-deficient aortas. The expression of eNOS protein detected using Western blotting was also significantly decreased in the perlecan-deficient aortas. We examined the role of perlecan in eNOS gene expression by creating perlecan knockdown human aortic endothelial cells using small interfering RNA (siRNA) for perlecan. Perlecan gene expression was significantly reduced in the perlecan siRNA-treated cells, resulting in a significant decrease in eNOS gene expression. Perlecan deficiency induced endothelial dysfunction, as indicated by a reduction in endothelium-dependent relaxation due, at least partly, to a reduction in eNOS expression. These findings suggest that perlecan plays a role in the activation of eNOS gene expression during normal growth processes.

Introduction

Vascular endothelial cells and vascular smooth muscle cells are two major research targets in the field of vascular physiology. The extracellular matrix in the vascular wall has recently attracted attention, as it not only provides structural support, but also modulates several cellular functions, including cellular adhesion, proliferation,

differentiation, and development (Pillarisetti 2000; Jiang and Couchman 2003; Iozzo 2005). The basement membrane is a thin sheet of the extracellular matrix that underlies the vascular endothelium and surrounds smooth muscle cells. Some of the key constituents of the subendothelial extracellular matrix are heparan sulfate proteoglycans (HSPGs). Perlecan (HSPG2) is a major HSPG in the basement membrane, with a molecular weight of over 400 kDa and a protein core consisting of five domains. It interacts with a number of extracellular matrix molecules, including laminin, collagen IV, fibronectin, fibrillin, and several growth factors, such as vascular endothelial growth factor (VEGF), fibroblast growth factors (FGFs), and platelet-derived growth factor (PDGF) (Iozzo 2005). Perlecan also interacts with plasma lipoprotein very low density lipoprotein (VLDL) (Hummel et al. 2004) and integrin cell surface receptor (Hummel et al. 2004). It also plays a role in a number of processes in the vasculature, including atherosclerosis, tumor angiogenesis, smooth muscle cell activity modulation, endothelial proliferation, and vascular development (Segev et al. 2004).

Others and we have previously reported that the homozygous deletion of *HSPG2* ($HSPG2^{-/-}$) in mice results in lethal chondrodysplasia and in cardiovascular abnormalities, such as transposition of the great arteries (Arikawa-Hirasawa et al. 1999; Costell et al. 1999, 2002). Perlecan deficiency ($HSPG2^{-/-}$) also causes perinatal lethal chondrodysplasia in humans (Costell et al. 1999; Arikawa-Hirasawa et al. 2001), suggesting a crucial role for perlecan in the development of cartilage and in the cardiovascular system. Mutations in the perlecan gene (*HSPG2*) have been identified in patients with Schwartz–Jampel syndrome, a nonlethal condition characterized by myotonia and mild chondrodysplasia (Nicole et al. 2000; Arikawa-Hirasawa et al. 2002; Stum et al. 2006). We investigated the role of perlecan in adult organs using a lethality rescued perlecan-null mouse model expressing recombinant perlecan specifically in cartilage ($HSPG2^{-/-}$-*Tg*) (Xu et al. 2010; Inomata et al. 2012; Ishijima et al. 2012; Kaneko et al. 2013). In addition to our lethality rescued $HSPG2^{-/-}$-*Tg* mouse model, studies employing mutant mice, such as heterozygous perlecan knockout ($HSPG2^{+/-}$) mice (Vikramadithyan et al. 2004) or heparan sulfate (HS)-deficient perlecan expressing mice (Tran-Lundmark et al. 2008), have provided further insights into the in vivo function of perlecan in adult tissues.

Endothelial dysfunction is considered to be a key variable in the pathogenesis of atherosclerosis and in its complications (Bonetti et al. 2002). The dysfunctional condition includes reduction in nitric oxide (NO) bioavailability, which may result in reduced vasorelaxation, thrombus formation, deposition of serum lipids, and the migration and proliferation of vascular smooth muscle cells (VSMCs), which leads to the formation of stenotic lesions in blood vessels (Cai and Harrison 2000). The regulation of vascular tone is the most widely studied aspect of the endothelial function, and NO is the major contributor to endothelium-dependent relaxation in large arteries. In the present study, we investigated the effects of perlecan deletion on endothelium-dependent vascular relaxation during the normal growth process and explored the mechanisms underlying the effects.

Materials and Methods

Animals

Perlecan-null ($HSPG2^{-/-}$) mice die perinatally due to premature cartilage development (Arikawa-Hirasawa et al. 1999; Costell et al. 1999). We previously created a perlecan transgenic mouse line (WT-Tg, $HSPG2^{+/+}$; *COL2A1-HSPG2*$^{Tg/-}$), which expresses recombinant perlecan in cartilage, using a cartilage-specific *COL2A1* promoter/enhancer (Tsumaki et al. 1999) to restore cartilage abnormalities. Subsequently, we created lethality-rescued mice ($HSPG2^{-/-}$ -Tg, $HSPG2^{-/-}$;*COL2A1-HSPG2*$^{Tg/-}$), by mating the transgenic mice with heterozygous $HSPG2^{+/-}$ mice (Xu et al. 2010). We maintained these mice on a mixed genetic background of C57BL/6 and 129SvJ. In the present study, we used $HSPG2^{-/-}$ -Tg mice for the experimental group and WT-Tg ($HSPG2^{+/+}$; *COL2A1-HSPG2*$^{Tg/-}$), mice (10 weeks of age) for the control group. All experimental procedures were performed in accordance with the guidelines for the care and use of animals at Juntendo University, Tokyo, Japan.

Measurement of changes in force in the mice aorta

The mice were sacrificed under anesthesia (Pentobarbital; 50 mg/kg, intraperitoneal administration). The descending thoracic aorta was isolated and cut into transverse rings (~2 mm in length), which were used to measure the changes in force. Care was taken not to touch the endothelial surface in order to preserve the functional endothelium. The techniques used to measure the changes in force were adapted from previously described methods (Iesaki et al. 1999; Sumiyoshi et al. 2008). Briefly, aortic rings were mounted on wire hooks attached to force displacement transducers (Nihon Kohden, Tokyo, Japan) and changes in the isometric force were recorded on a thermal recorder (Rika Denki, Tokyo, Japan). The rings were incubated in individually thermostated (37°C)

10-mL baths filled with oxygenated Krebs bicarbonate buffer (118 mmol/L NaCl, 4.7 mmol/L KCl, 1.5 mmol/L $CaCl_2$, 25 mmol/L $NaHCO_3$, 1.1 mmol/L $MgSO_4$, 1.2 mmol/L KH_2PO_4, and 5.6 mmol/L glucose at pH 7.4). An optimal passive tension of 0.5 g was applied to the rings throughout the experiment. The vascular rings were initially exposed to high-K^+ Krebs bicarbonate buffer, containing 60 mmol/L KCl in place of NaCl to produce maximal force and to enhance the reproducibility of subsequent contractions. After a wash out of high-K^+ buffer, the vessels were submaximally contracted with 1 μmol/L phenylephrine. Once a steady-state level of contraction was achieved, endothelial-dependent relaxation and endothelial-independent relaxation were elicited by the administration of increasing concentrations of acetylcholine (ACh) and sodium nitroprusside (SNP), respectively. Relaxation was expressed as the percent change in the steady-state level of contraction. Comparisons between groups were made with two-way reported measure ANOVA.

Quantitative real-time polymerase chain reaction

Total RNA was isolated from mouse thoracic aortic tissue or human aortic endothelial cells (HAECs; LONZA, Walkersville, MD) using TRIzol reagent (Life Technologies, Carlsbad, CA), according to the manufacturer's instructions. cDNA was generated from 1 μg of total RNA with M-MLV reverse transcriptase (Promega, Madison, WI) and a random primer (TAKARA, Siga, Japan). SYBR Green was used for detection, and RNA expression was normalized to that of the housekeeping gene β-actin for mouse, GAPDH for human. In the graph, the eNOS, von Willebrand factor, and perlecan (HSPG2) expression levels are indicated as relative to β-actin or GAPDH. The PCR reaction was carried out in an ABI Prism® 7500 Fast Sequence Detection System (Life Technologies). The primer sequences were as follows: For the mouse tissue, mouse eNOS forward 5′-CTGGCAGCCCAAGACCTA-3′, mouse eNOS reverse 5′-GTGACATCGCCGCAGACAA-3′, mouse von Willebrand factor forward 5′-GATGCCCCAGTCAGCTCTAC-3′, mouse von Willebrand factor reverse 5′- TCAGCCTCGGACAACATAGA-3′, mouse β-actin forward 5′-TGGAATC CTGTGGCATCCATGAAAC-3′, mouse β-actin reverse 5′-TAAAACGCAGCTCAGTAACAGTCCG-3′. For the HAECs, human HSPG2 forward 5′-GGCTGAGGGCATACGATGGCT-3′, human HSPG2 reverse 5′-CCCACTGC CCAGGTCGTCTCC-3′, human eNOS forward 5′-CCCTT CAGTGGCTGGTACAT-3′, human eNOS reverse 5′-CACGATGGTGACTTTGGCTA-3′, human GAPDH forward 5′-ACCACAGTCCATGCCATCAC-3′, human GAPDH reverse 5′-TCCACCACCCTGTTGCTGTA-3′

Western blotting

Thoracic aortic tissue was isolated and then homogenized in cold lysis buffer, and the lysate was centrifuged at 16,000 *g* for 15 min at 4°C. The lysis buffer contained 50 mmol/L Tris-HCl (pH 7.2), 150 mmol/L NaCl, 1% Nonidet P-40, 1% sodium deoxycholate, 0.1% SDS containing protease, and phosphatase inhibitor cocktails (Complete Protease Inhibitor Cocktail and PhosSTOP; Roche, Rotkreuz, Switzerland). The protein concentration was determined using a BCA protein assay kit (Thermo Scientific, Rockford, IL) and then solubilized in NuPAGE® LDS sample buffer (Life Technologies) containing dithiothreitol. The samples (15 μg/lane) were resolved via electrophoresis on 4–12% SDS-PAGE gels, and then transferred to a PVDF membrane (Life Technologies, Carlsbad, CA). After blocking with PVDF blocking reagent (TOYOBO, Osaka, Japan), the membrane was incubated with primary antibodies in blocking reagent overnight. After washing, the membrane was incubated with horseradish peroxidase (HRP)-conjugated secondary antibodies in blocking reagent and visualized with SuperSignal®West Dura Extended Duration Substrate (Thermo Scientific, Rockford, IL). Specific bands were quantitated using the ImageJ software program. In the graph, the eNOS protein level is indicated as relative to β-actin. The experiments were performed at least three times using different sibling pairs of animals. The antibodies were prepared as follows: the primary antibodies, mouse anti-eNOS/NOS type III antibodies (BD Biosciences, Franklin Lakes, NJ) or mouse anti-β-actin antibody (Santa Cruz Biotechnology, Inc., Dallas, TX) were diluted at 1:1000 or 1:5000 in blocking reagent. The secondary antibodies, anti-mouse IgG HRP-conjugated secondary antibodies (GE Healthcare, Little Chalfont, UK) were diluted at 1:5000 in blocking solution.

Cell culture and small interfering RNA (siRNA)

Human aortic endothelial cells (HAECs) were grown using the Endothelial Cell Growth Media Kit (EGM-2 BulletKit; LONZA), and plated at a density of 2×10^5 cells on 6-well plates. Perlecan siRNA and control siRNA were purchased from Santa Cruz Biotechnology. HAECs were transfected with either perlecan or control siRNA, according to the manufacturer's recommendations. Forty-eight hours after transfection, knockdown efficiency was assessed using quantitative RT-PCR (qPCR), as described above. For perlecan rescue experiments, we used the recombinant perlecan protein (rPerlecan) kindly provided by Dr. Sasaki. The recombinant perlecan was purified from the condition media of 293

cells transfected with a perlecan cDNA expression vector (Noonan et al. 1991; Costell et al. 1997; Xu et al. 2010). The full-length perlecan cDNA (Ishijima et al. 2012) was cloned into the PCEP4-Mul-PURD expression vector (Hozumi et al. 2006), which contains sequences for the CMV promoter, multiple cloning sites, BM40 signal peptide (Hozumi et al. 2006). A twenty-four well tissue culture plate was coated with rPerlecan (20 μg/mL) in PBS, including 1 mmol/L $CaCl_2$ and 0.5 mmol/L $MgCl_2$ at 4°C for 48 h. After the plate was washed twice with PBS, HAECs treated with Perlecan siRNA or Control siRNA, as described above, were plated at density of 3×10^5 cells on the Perlecan or a control plate and cultured for 36 h. The eNOS RNA expression was analyzed using qPCR.

Heparinase III digestion of HAECs

Cell surface heparan sulfate chains of HAECs were digested by heparinase III as described method (Kerever et al. 2007) with some modifications. HAECs were incubated with 5 mU/mL of heparinase III (Sigma-Aldrich, St. Louis, MO) in 50 mmol/L HEPES buffer (pH 7.0), containing 100 mmol/L NaCl and 1 mmol/L $CaCl_2$ at 37°C for 1 h. After the incubation, the heparinase III solution was removed and the cells were cultured with the growth media. We confirmed successful heparinase III digestion using immunostaining. A time course of the eNOS RNA expression was performed using qPCR as described above.

Immunostaining

HAECs were plated at density of 3×10^5 cells on Type-1 collagen-coated 8 well chambers and cultured for 48 h. After heparinase III digestion for 1 h, the cells were fixed immediately (time point 0) or 24 h later (time point 24 h) with 4% paraformaldehyde at room temperature. Nonspecific binding was blocked with 0.2% gelatin/PBS for 10 min and cells were incubated with anti-heparan sulfate antibody (10E4 epitope) antibody or anti-Δheparan sulfate (3G10 epitope) antibody (Seikagaku Corporation, Tokyo, Japan) at 1:400, and anti-perlecan (clone A7L6) (Chemicon, Temecula, CA) antibody at 1:400 in 0.2% gelatin/PBS at 4°C overnight. Following a wash with PBS, the cells were incubated with goat anti-mouse IgM alexafluor 488 and goat anti-rat IgG alexafluor 546 (Molecular Probes, Invitrogen Corporation, Carlsbad, CA) at 1:400 in 0.2% gelatin/PBS for 1 h. The cells were washed and then incubated for 10 min in bis-benzimide (1:5000, Molecular Probes, Invitrogen Corporation). After extensive washes, cells were mounted in fluoro-gel with Tris buffer (Electron Microscopy Sciences, Hatfield, PA). Images were taken using a Leica TCS-SP5 LSM confocal microscope.

Statistical analysis

The data are presented as the mean ± SEM. Comparisons between groups were made with two-way reported measure ANOVA and with the unpaired t-test. A P value of <0.05 was considered to be statistically significant.

Results

HSPG2 deletion decreases the relaxation of mouse aorta

An endothelium-dependent relaxation of the mouse aorta was elicited by ACh. Aortic relaxation in response to ACh was significantly reduced in the *HSPG2*$^{-/-}$-Tg aortas compared to that of the control aortas, resulting in the downward shift of the concentration-response curve (Fig. 1A). On the other hand, the endothelium-independent relaxation elicited by exogenous nitric oxide donor

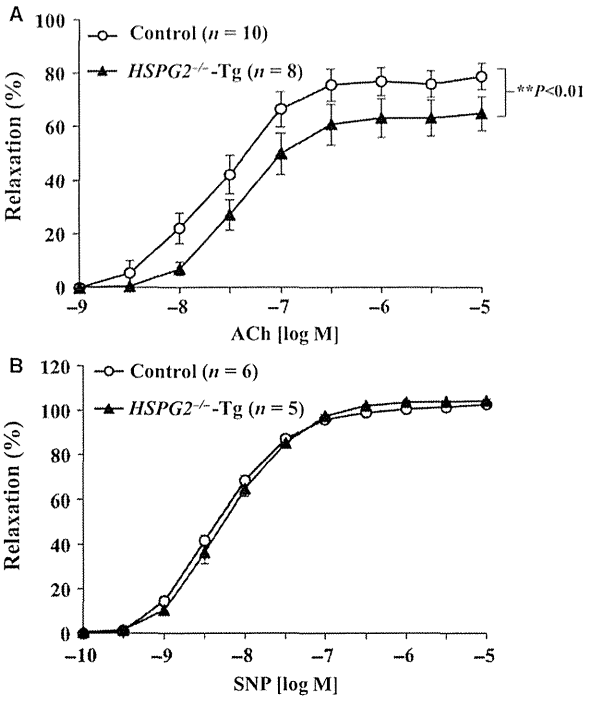

Figure 1. *HSPG2*$^{-/-}$-Tg aortas have a reduced relaxation in response to ACh or SNP. The aortic rings were precontracted with 1 μmol/L phenylephrine (PE), and increasing concentrations of (A) acetylcholine (ACh) or (B) sodium nitroprusside (SNP) were added. The degree of relaxation is expressed as the percent relaxation of the PE-induced tone (The bars indicate the mean ± SEM, n = 5–10).